12-2016

Synthesis, Characterization, and Fabrication of All Inorganic Quantum Dot LEDs

Haider Baqer Salman
University of Arkansas, Fayetteville

Synthesis, Characterization, and Fabrication of All Inorganic Quantum Dot LEDs

A thesis submitted in partial fulfillment
of the requirements for the degree of
Master of Science in Microelectronics-Photonics

by

Haider Baqer Salman
University of Baghdad
Bachelor of Science in Electronic and Communication Engineering, 2004

December 2016
University of Arkansas

This thesis is approved for recommendation to the Graduate Council.

Dr. Omar Manasreh
Thesis Director

Dr. Rick Wise
Ex-Officio Member

Dr. Simon Ang
Committee Member

Dr. Jiali Li
Committee Member

The following signatories attest that all software used in this thesis was legally licensed for use by Haider Baqer Salman for research purposes and publication.

Haider Baqer Salman	Dr. Omar Manasreh, Thesis Director

This thesis was submitted to http://www.turnitin.com for plagiarism review by the TurnItIn company's software. The signatories have examined the report on this thesis that was returned by TurnItIn and attest that, in their opinion, the items highlighted by the software are incidental to common usage and are not plagiarized material.

Dr. Rick Wise, Program Director	Dr. Omar Manasreh, Thesis Director

Abstract

Quantum Dot LEDs with all inorganic materials are investigated in this thesis. The research was motivated by the potential disruptive technology of core shell quantum dots in lighting and display applications. These devices consisted of three main layers: hole transport layer (HTL), electron transport layer (ETL), and emissive layer where the emission of photons occurs. The latter part was formed of CdSe / ZnS core-shell quantum dots, which were synthesized following hot injection method. The ETL and the HTL were formed of zinc oxide nanocrystals and nickel oxide, respectively. Motivated by the low cost synthesis and deposition, NiO and ZnO were synthesized following sol-gel method and deposited using spin coating. The anode of the device was a commercial slide of indium tin oxide deposited on glass substrate while the cathode was a 100 nm aluminum layer that was deposited using an Auto 306T Edwards thermal evaporator.

In this research, Raman spectroscopy, micro-photoluminescence spectroscopy, absorbance spectroscopy, X-ray diffraction (XRD) spectroscopy, and atomic force microscopy, were used to characterize the materials. Three sharp peaks were observed in the XRD measurements of the NiO thin film related to three planes and indicated a proper level of crystallinity. The AFM image of the same material indicated a roughness RMS value of 2 nm which was accepted for a device fabrication.

The photoluminescence spectrum exhibited a peak at 515 nm for the quantum dots and a peak at 315 nm for the ZnO nanocrystals. The narrow shape of these spectra proved a limited amount of size variation. The transfer characteristics of the fabricated device indicated that the current density ramped up producing green light when the voltage was higher than 5 V to reach 160 mA cm^{-2} at 9 V.

Acknowledgements

Firstly, I would like to thank my parents for their support and encouragement, which have been a great motivation for me to finish the research.

Secondly, I would like to thank my graduate advisor, Dr. Omar Mansreh, for his guidance and support throughout my whole research, and for giving me the opportunity to join his research group.

Also, I'm very grateful to Professor Ken Vickers for helping me to join the MicroEP program and for his valuable mentorship during my first semester.

I would like to thank Dr. Rick Wise, the director of the microEP program for his help and guidance, and also Dr. Simon Ang and Dr. Jiali Li for being members of my committee.

Finally, I would like to thank my lab-mates Ramesh Vasan, Mohamed Marie, and Ahmed Nusair for their support in completing my project.

Table of Contents

List of Figures

Chapter 1 Introduction

During the past years, quantum dot LEDs (QD-LEDs) gained the interest of researchers as a potential alternative for the organic LEDs in display technology applications [1], [2], [3]. Narrow bandwidth, high quality tunable color and high electrochemical stability are the most important features of the QDs [1], [2], [3]. With colloidal QDs, it is possible to produce a photoluminescence spectrum that is half the width of that produced by the regular organic LEDs [1], [2]. Such narrow spectrum is an indication of a pure color, which is a result of high QD size uniformity where the size variation can reach down to 4% to 5% [1], [3], [4]. For long life devices, it is crucial to use materials with high electrochemical stability. Unlike organic LEDs, quantum dots have high electrochemical stability that makes them alternative competitive materials for long life display devices [1], [2]. However, some hurdles still exist, among which is the relatively low efficiency which is <1% for all inorganic LEDs and 18% for hybrid LED [4]. In addition, the mechanism of the device and the theoretical concepts are not completely understood yet [2], [4], [5], [6], [7]. Quantum dots are prepared by epitaxial and colloidal growths. The latter method is preferred in optoelectronic applications because of the high mono-dispersity it offers.

1.1 Quantum Dots Properties

Quantum dots are semiconductors shaped as crystals in which charge carriers are confined in three dimensions. Each single crystal contains hundreds, to thousands, of atoms [1], [8]. Because of the unique optical properties that QDs have, they have been expanding in the market in different kinds of optoelectronic applications [2]. The first attempt of marketing QDs was in optical filters where blue light, mostly produced by GaN LEDs, is absorbed and reemitted

at longer wavelengths [2], [6]. The size of the QDs controls the color of the emitted light so that different colors can be produced by the same QDs but with different sizes. Usually the size of a QD ranges between 1.7 nm for blue light and 5 nm for red light [1]. High color purity emitted by a certain material is an interpretation of the width of the emission spectrum produced by that material. The emission spectrum of QDs can have a full width at half-maximum (FWHM) as narrow as 20 nm [4], [9]. The narrow bandwidth and the high quality tunable color of the colloidal quantum dots make them a desired material in lighting and display applications [2], [9]. There are two main differences between spectrums of the QDs and that of the organic dye, the closest competitor in display application. Firstly, the width of the QDs emission spectrum is almost half than that of the organic dye used in organic LEDs, secondly, the absorbance intensity of the QDs increases with shorter wavelengths, which makes it possible for more than optical excitation to happen in the same time using the same blue or UV light source [2].

The origin of the unique characteristics that QDs have comes from the concept of confinement. This concept means that the carriers inside the dots have more spacing between the discrete energy levels [1], [10]. The confinement effect takes place when the diameter of the quantum dots becomes close to the distance between an electron and a hole known as Bohr radius which can be calculated from the following equation:

$$r = \in a^{\circ} m^{\circ} / m^{*} \qquad \text{(Equation 1.1)}$$

where r is Bohr radius, $\in$ is the dielectric constant of the material, a° is Bohr radius of a hydrogen atom, m° and m^{*} are the electron basic and effective mass, respectively. From the previous equation, it can be concluded that there is a wide range of distance at which the confinement effect starts to appear. For example, the confinement appears in CdS QDs at a radius of 2 nm while it does not appear until 100 nm in PbTe QDs [1]. On the other hand, the QDs of two different materials that have the same size experience different level of confinement.

For example, the confinement energy of a 3 nm CdSe is half than that of PbSe, which has the same size [1].

1.2 Core Shell Quantum Dots

The high surface to volume ratio of the quantum dots leads to the fact that a large number of the atoms of the QDs exist on the surface. For example, almost 40% of the atoms exist on the surface of a PbSe single QD of 5 nm has [1], [9], [10]. Thus, the number of the potential dangling bonds that can act as surface traps is high. In general, dangling bonds are unsatisfied covalent bonds that act as a state that traps electrons or holes since the energy of these states lie within the band gap of the QDs. Usually, the organic ligands that are used in the synthesis procedure function as stabilizer and passivate the QD surface [1], [2], [4], [11]. However, some of the dangling bonds can still exist even after the organic ligands passivation. In addition, the passivation increases the stability of the QDs by preventing further aggregation, which leads to increasing the QD size.

Coating the QDs with another inorganic material is an effective approach to improve the passivation and results in what is known as core-shell quantum dots [1],[10],[12]. Core-shell QDs are classified into three types based on the material band gaps and band alignment. These types are: type I, type II, and type II reverse. In type I, the band gap of the shell material is higher than that of the core material [1], [12]. In this type, electrons are confined in the core because the conduction band level of the core is lower than that of the shell. In addition, holes are also confined in the core because the valence band level of the core is higher than that of the shell. CdSe / ZnS and CdSe / CdS are common examples of type I. In type II, both conduction and valence band levels of the core are either lower or higher than those of the shell [13]. Such structure has either electrons or holes to be confined in the core [12], [13]. A common example

of this type is CdSe/ ZnTe where electrons are confined in the core because the conduction band level of the CdSe is lower than that of the ZnTe. In the same time, holes are confined in the ZnTe shell because its valence band level is higher than that of the CdSe. In Type I reverse, the conduction and the valence band levels of the shell are located inside the band gap of the core, which makes both electrons and holes confined in the shell. Examples of the last type are ZnSe/CdSe and CdS/HgS.

Regardless of the type, adding shells causes a red shift to the PL spectrum of the QDs compared with the spectrum of the mere dots [1], [12], [14], [15]. The reason behind the red shift is the leakage of the excitons to the shell material [14]. Coating cores with shells increases the passivation which leads to higher PL intensity and this is the main purpose of doing so, but at the same time it lowers the confinement of the carriers which leads to the red shift [14], [16]. In the mere dots, the wave function of the electron, exists in the whole space of the core and partially leaks into the organic ligand, but there is a less probability of holes to leak into the surrounding ligand because the hole mass is heavier than that of the electron [1], [12] [17]. In core shell quantum dots, the probability of tunneling into the shell material is higher with electron waves than with hole waves. The lower the confinement, the lower the excitement energy states, which means a red shift in the PL spectrum. Red shift is observed in all the types of QDs, but in different levels. It is small in Type-I and big in Type-I reverse. Red shift also depends on the size of the core. In small cores, the leakage of the carriers has a large effect on the confinement energies, which leads to large amount of red shift.

As mentioned earlier, coating mere dots with shells reduces the trap states and increases the intensity of the emission spectrum, since there will be less non-radiative decay. The latter feature is the reason why core shell QDs is preferred in lighting applications. As an example of the improvement in the PL spectrum, CdSe/ZnS QDs experience an increase in the emission

intensity that can reach up to 4 times that obtained from CdSe mere dots [1]. In addition, over-coating of QD cores with shells introduces a high barrier to oxygen diffusion, which prevents the photo oxidation and increases the photo-stability.

1.3 Lattice Mismatch

The increase in the emission spectrum is accompanied by a lattice mismatch caused by the difference in the composition of the materials between the core and the shell. Lattice mismatch plays an important role in limiting the efficiency of QD-LEDs [18], [19], [20]. The difference in the composition of the core and the shell produces strain at the core shell interface, which leads to a shape deformation of the QDs. Based on the value of the lattice strain energy density, the shell surface might be affected having thin and thick areas [20]. It is reported that the value of the lattice strain energy density should be kept below 0.85 eV/nm^2 to ensure that the QDs optical properties do not change [18].

Usually, the lattice parameter of the core is smaller than that of the shell, which leads to an isotropic compression applied on the core and both radial compression and tangential tension applied on the shell. Small cores can be compressed highly enough not to exceed the critical value of the strain energy density [18], [20]. Smith et al. investigated the effect of the lattice stain on CdTe/ ZnSe core shell QDs and confirmed that big changes to the energy levels of the conduction and valence bands can happen prompted by the lattice strain [20].

Figure 1.1 illustrates how the lattice strain shifts the conduction and valence bands for different sizes of CdTe/ZnSe core shells QDs. The reason behind this effect is that for group II-VI and III-V that have zinc-blende crystals, the compressive force raises the band gap energy.

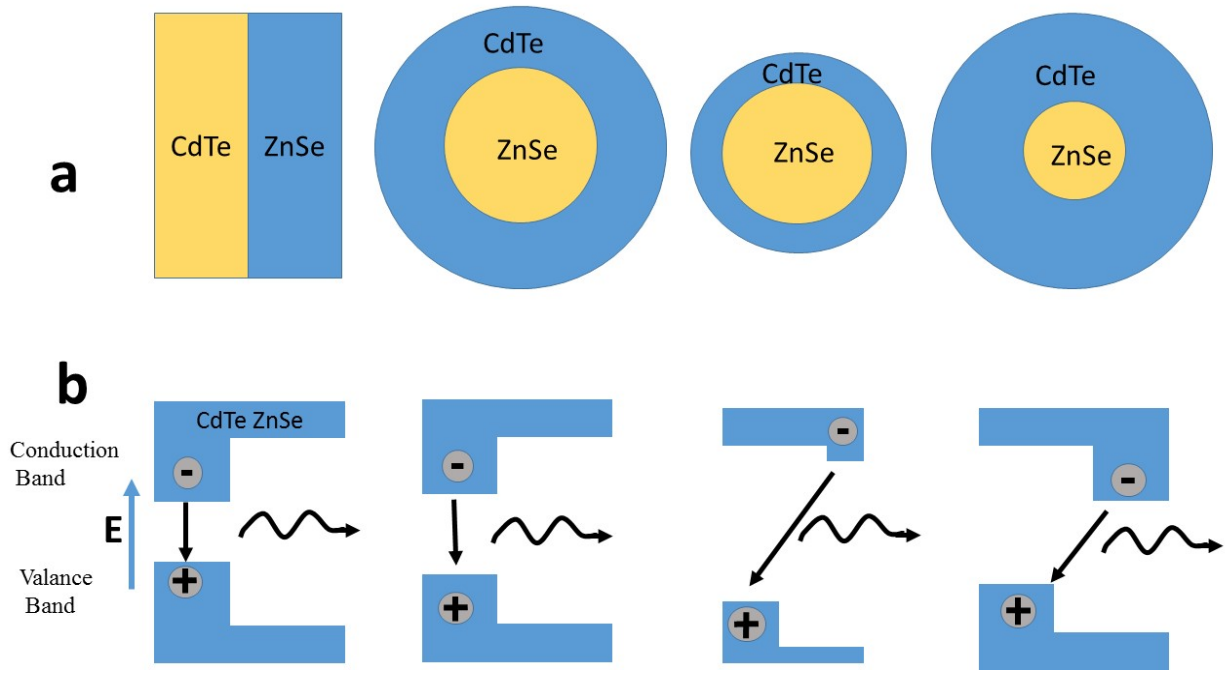

Figure 1.1: Schematic diagram of the effect of the lattice mismatch strain on the energy bands of core shell QDs. (a) CdTe/ ZnSe core shell QDs under stain conditions. (b) Conduction and valence band affected by the lattice strain.

For the same types of materials, the tensile strain lowers the band gap energy. Thus for the case of CdTe/ZnSe, the core is subjected to a compression so its conduction band gap gets higher, while the ZnSe is subjected to a tensile stain, so its conduction band gets lower. This change in the energy of the conduction and valence bands leads to a change in the type of the QDs from type I to type II [20].

Annealing at higher temperatures is an approach to overcome the lattice mismatch where high temperature annealing allows inter-diffusion between the materials of the core and the shell creating an alloy intermediate region between them. With large alloy regions, the gradual change in composition from the core to shell materials reduces lattice mismatch strain and provides high photoluminescence quantum yield (PL QY) [18]. However, the problem with this

method is the aging of the nanocrystals (NCs) that takes place as a result of annealing which increases the range of the NC size distribution.

1.4 Quantum Dot LED Mechanism

Quantum dot LEDs consist of three main parts: emissive layer which is the quantum dots layer, hole transport layer, and electron transport layer as shown in Figure 1.2.

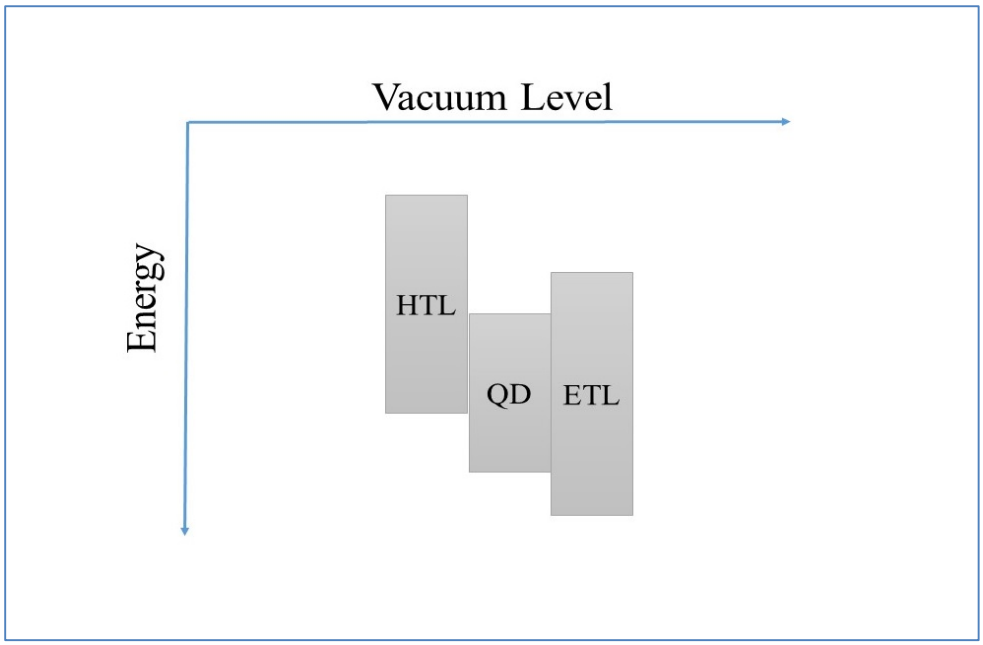

Figure 1.2: Basic structure of QD-LED illustrates the three main layers HTL, QDs, and ETL with their relative band alignment.

The whole mechanism of how QD-LEDs work is not understood yet but it is suggested that holes and electrons are produced by either direct injection method from the HTL and the ETL, respectively, to the emissive layer or by Forster transfer mechanism. The combination between carriers excites the QDs to a higher state before they relax back to the initial states emitting photons with an energy level that is equal to the band gap of the QDs. This process needs a balance in the injection rate of the holes and the electrons. Without such balance,

carriers gather on the QDs making them either positively or negatively charged, which leads to non-radiative recombination or PL blinking [2], [21].

In QD-LEDs, fluorescence intermittency or blinking is the continuous switching between the On and the Off states in the photoluminescence. Up to now, there is no unified theory that can precisely explain the mechanism of this observation. In general, the off state is believed to occur when photo-charged or ionized QDs experience a strong non-radiative decay. On the other hand, there is a possibility that the trapped carriers neutralize the QDs allowing an emission to take place, which is the On state of the blinking. Up to now, it is still difficult to balance the injection rate from both layers because of the relatively high hole barriers compared with the electron barriers for most of the materials that are currently being used in fabricating the QD-LEDs. Thus, it is crucial to optimize the energy band alignment by selecting materials that offer equal barriers for both electrons and holes.

1.4.1 Direct Injection Method

In this method, electrons and holes driven by the bias voltage are directly injected from the electron and hole injections layers to recombine in the QDs layer and emit photons. As stated before, the mechanism is not clearly understood, but for the QD-LEDs with all inorganic materials, it is believed that the direct injection method is dominant [1], [4]. QD charging is more likely to take place with this method of injection. Hybrid QD-LEDs with organic transport layers were designed to overcome the problem of QD charging by allowing the second type of injection known as FRET.

1.4.2 Forster Resonance Energy Transfer FRET in QDs-LEDs

Forester Resonance Energy Transfer, referred to as FRET, is the second method of charge injection. The mechanism of the FRET in QD-LEDs is illustrated in Figure 1.3. In general, FRET is a way of non-radiative energy transfer between two molecules: donor and acceptor [22].

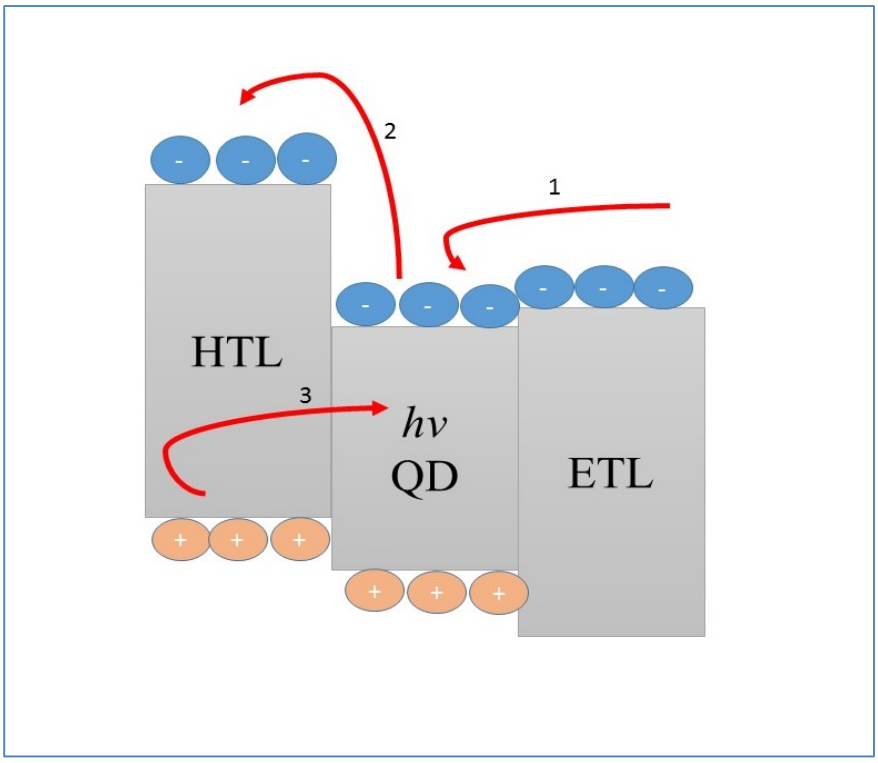

Figure 1.3: Schematic diagram illustrating the FRET mechanism between the carriers of a QD-LED.

The efficiency of the energy transfer is inversely proportional to the sixth power of the distance between the donor and the acceptor, which makes it strongly sensitive to small changes in distance [22]. For a FRET to occur, the distance between the donor and the acceptor should be very small. In addition, there must be an overlap between the absorption and the emission spectrum of the donor and the acceptor, respectively [22]. An exciton is formed on the organic molecules at the vicinity of the QDs, then the energy of the formed excitons is transferred to the

QDs by FRET mechanism [5] ,[23], [24]. In the past years, researchers focused on utilizing this mechanism to increase the efficiency of the QD-LEDs.

1.4.3 Efficiency Calculations

Up to now, the reported External Quantum Efficiency EQE of QD-LED is 1%, which is very low compared with what is obtained from the hybrid QD-LED or the QLED that can reach up to 24% [25]. The EQE of the device is defined in the following equation:

$$EQE = Ne/Np \qquad \text{(Equation 1.2)}$$

where *Ne* and *Np* are the number of injected electrons and the emitted photons per unit of time respectively. The external quantum efficiency depends also on the luminescent quantum yield QY, which is the probability of emitting a photon by an exciton [21].

Quantum yield can be represented in the following equation:

$$QY = (1 - N)k\tau \qquad \text{(Equation 1.3)}$$

where τ is the life time of an excitons, $k\tau$ is the radiative decay rate of an exciton, and *N* is the fraction of QDs that are emitting during the operation of the device. When charges are injected into the QD layer, N increases reducing the quantum yield [21]. Some of the injected charges are trapped and accumulated on the QD surface [1], [2], [11]. The latter process causes the exciton to transfer their energy to the charges on the QDs by a non-radiative mechanism. As discussed earlier, coating QDs with appropriate cores reduce the charging process and thus results in higher QY [21]. Charging QDs is the driving force behind Auger recombination that is believed to have a major influence on reducing the efficiency of QD-LEDs when operating at a high value of current [26]. Auger recombination is a process that involves three carriers in which the energy of two opposite carriers (electron and hole) is transferred to the third carrier.

The third carrier is excited to higher states before going down again without producing photon. The last carrier can either be an electron or a hole for negative trions or biexcitons, respectively [21], [26], [27].

1.5 Inverted Structure

Inverted structure is the second form of QD-LED, in which the position of the HTL and the ETL are reversed so that the electrons are injected from the anode and transported to the emissive layer through the ETL. Similarly, holes are injected from the metallic cathode and transported through the HTL [1], [28], [29]. It is believed that the electroluminescence of the inverted structure is higher than that of the conventional structure because the injection rate of electrons and holes is more balanced [28], [29]. As stated previously, the main reason behind the imbalance of the electrons and holes injection is the high barrier to holes compared with electrons. This problem is partially solved by using the inverted structure because there is a high barrier for the electrons as well as for the holes. Usually MoO_3 is used in this structure as a hole injection layer that reduces the barrier for the holes and as a barrier for the electrons in the same time. Bhaumik et al. reported obtaining higher electroluminescence with inverted structure using MoO_3 as a hole injection layer, ZnO, and graphene oxide (GO) as an electron and hole transport layer, respectively.

Chapter 2 Materials Synthesis and Device Fabrication

This chapter illustrates the methods of the colloidal synthesis used to prepare the materials of the device, and the significance of using such. It also, explains the step of the device fabrication.

2.1 Sol-Gel Method

Sol-gel is a common method in chemistry used to prepare solid materials from solutions by precipitating the solid from the sol. A sol is a solution that contains two phases: continuous and dispersed which are liquid and solid [30],[31]. The continuous phase in a gel is solid while the dispersed phase is liquid. Figure 2.1 illustrates the main steps of a general sol-gel synthesis.

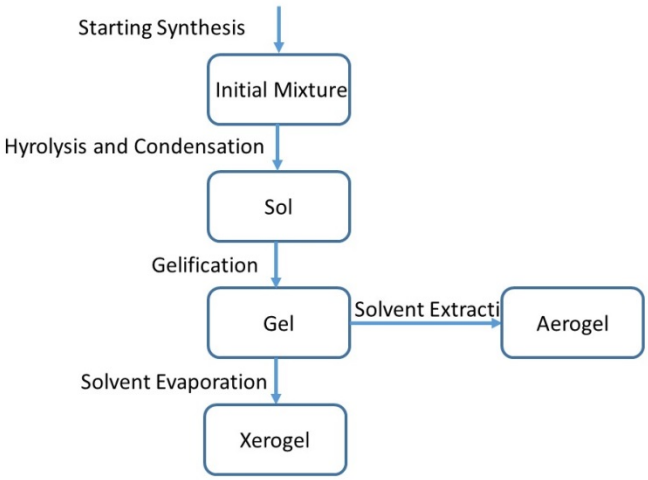

Figure 2.1: Schematic diagram illustrating the basic steps of Sol-Gel synthesis method.

When the nanoparticles inside a liquid aggregate to form a network of particles, the sol behaves as a precursor for the particle aggregation, which is transformed to gel making the viscosity increase. The reaction strongly depends on the temperature that affects the rate of the

nanoparticle formation and assembly where, at higher temperatures, the reaction can be fast so that it forms clumps instead of uniform network of nanoparticles [31].

This method was followed in synthesizing the metal oxide transport layers of the device.

2.2 Hot Injection Method

In this method it is possible to obtain highly mono-disperse QDs [1], [32]. The nucleation is triggered by swiftly injecting a precursor at the room temperature into a hot solution at 300 ^{o}C. After a few seconds from injecting the precursor, the temperature of the whole mixture drops to about 170 ^{o}C. This drop in temperature prevents the formation of new nuclei and instead it results in monodisperse nuclei with precursors. The existing nuclei grow forming nanocrystals when the temperature increases (still below 300 ^{o}C) but without the formation of new nuclei as shown in Figure 2.2.

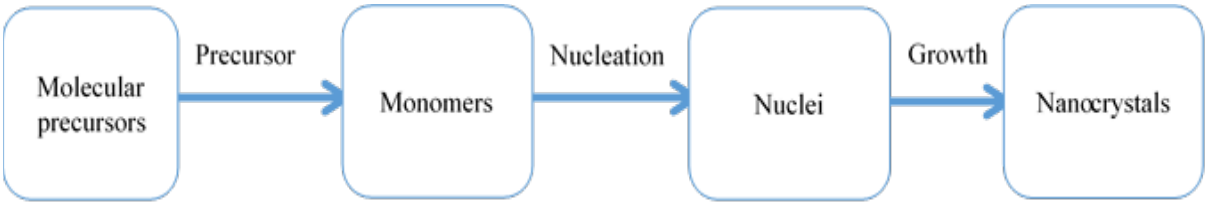

Figure 2.2: Flow chart illustrating the main stages of QDs synthesis by hot injection method.

The growth temperature controls QD size i.e. at higher temperatures, the resulting QDs are bigger. These steps are controlled by the existence of stabilizers during the reaction. The latter are surfactants that cap the surface of the nanocrystals which is an important process to stabilize the resulting QDs and make them form wurtzite lattice with minimum defects [32].

2.3 Nickel Oxide Thin Films

Among the materials that are used as hole transport layer, PEDOT:PSS represents one of the most common options. The advantages of using this material is that it can produce less rough thin film morphology when deposited on the indium tin oxide (ITO) slides where high roughness can decrease the device performance [33]. It is reported that the roughness of the HTL is mostly caused by the ITO substrate, but good HTL such as PEDOT:PSS can passivate this effect and RMS roughness value of 0.9 nm can be obtained [33]. However, the relatively high acidity of this materials makes it easy to degrade and difficult to use for long life devices [34], [35]. PEDOT:PSS has a high PH value and acidity nature which is a limiting factor for transparent conductive materials that can be easily etched [34], [35]. Also, this material is hygroscopic which means that it is a good moisture absorbent which causes erosion in the transparent conductive material substrate [36]. This erosion causes water to damage the device allowing diffusion between the different layers [36]. All the above problems with PEDOT: PSS encouraged more research on different materials including NiO.

Nickel oxide is a p-type semiconductor that can be used as a hole transport layer for both QD-LEDs and solar cells. It has a wide band gap ($E_g > 3$ eV) and high transmittance that makes it a good option for use in optoelectronic devices [37], [38], [39]. The high electrochemical stability of NiO is its main advantages over PEDOT:PSS, which makes it a good option for long life devices [37], [38], [39]. The reason behind the p-type nature of NiO is basically the two positive charges produced by the NiO^{+2} vacancy [40],[41],[42].

Nickel oxide was prepared by sol-gel methods reported in literature. One mol of nickel acetate tetra hydrate was dissolved in 10 ml of ethanol under room temperature. Then, an equimolar amount of diethanolamine was added to the solution before leaving it under stirring for two hours. The result was a green solution nickel hydroxide as shown in Figure. 2.3, which

turned to nickel oxide after the annealing process, which was performed in a furnace at 500 ^{o}C. The other details of depositing the NiO thin films will be in the device fabrication section.

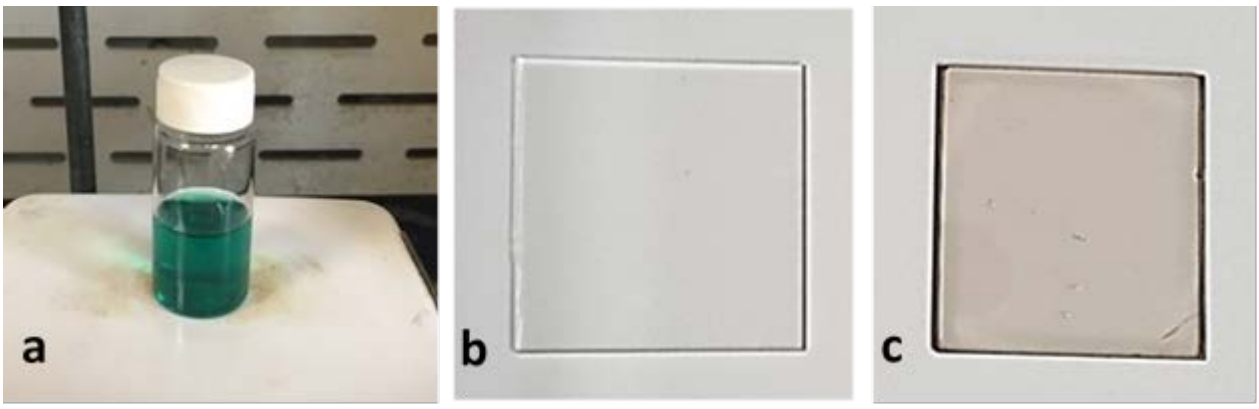

Figure 2.3: Nickel oxide synthesis and deposition: (a) nickel hydroxide solution, (b) indium tin oxide substrate, and (c) resulting NiO thin film after depositing the nickel hydroxide over the ITO substrate and annealing at 500 ^{o}C.

2.4 Zinc Oxide Nanocrystals

Zinc oxide is one of the most studied materials in optoelectronics and biomedical applications due to its abundance and easy synthesis [43], [44],[45]. The binding energy of ZnO at room temperature is reported to be 60 eV while its energy band gap is reported to be 3.37 eV at room temperature making the emission spectrum of this materials lie within the ultra violet region of light [46]. Naturally, ZnO is an intrinsic n-type semiconductor due to the existence of defects that change Fermi level accordingly [46], [43]. These defects must behave like donors to participate in the negative charges conductivity.

To understand the nature of the conductivity in an intrinsic semiconductor, two key features of impurities need to be identified: the formation energy of the impurities and their positions (deep or shallow). To have a high number of conducting impurities, the formation energy should be low, while only shallow impurities can participate in the conductivity of the

material [43]. Previously, oxygen vacancies were thought to have a big role in creating the intrinsic carriers of ZnO. However, recent studies found that the oxygen vacancies are deep donors instead of shallow, which makes them unable to be part of ZnO conductivity regardless of the fact that among donors, oxygen vacancies need the least amount of energy to be created [43], [47],[48],[49]. The defects that have high formation energy are oxygen interstitials, oxygen antisites, zinc interstitials and zinc antisites. On the other hand, the formation energy of zinc vacancies is low but they are but they are not donors. To summarize the above, the n-type nature of zinc oxide cannot be attributed to one single type of impurity. In this research, zinc oxide nanocrystals were synthesized using sol-gel method resulting white nanocrystals as shown in Figure 2.4 (a).

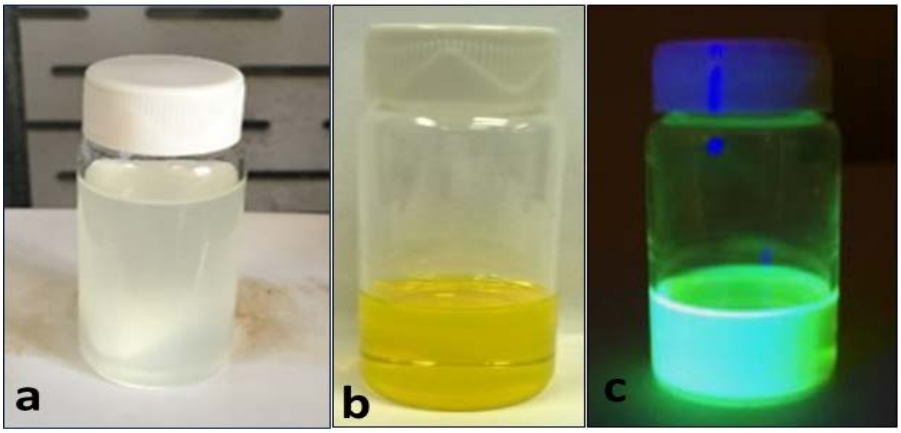

Figure 2.4: Nanocrystals synthesized in the lab after purification. (a) ZnO NCs in solution. (b) CdSe QDs in solution under white light, and (c) CdSe QDs in solution under UV light.

The synthesis was initiated by dissolving 1 mol of zinc acetate in 50 ml of ethanol at 60 ^{o}C until it completely dissolved. In a separate beaker, 3.3 ml of tetramethylammonium was dissolved in 16 ml of ethanol. Under stirring, the second solution was slowly added to the first. After 30 minutes, the final mixture was cooled down to the room temperature. The resulting nanocrystals were purified by using the centrifuge after adding toluene and methanol to

precipitate the nanocrystals. Then, the precipitated nanocrystals were put under vacuum for 24 hours to completely dry. The dried crystals were dispersed in butanol for the deposition process.

2.5 Cadmium Selenide / Zinc Sulfide Core-shell Quantum Dots

One of the most commonly used QDs in optoelectronic application is CdSe/ZnS core shell quantum dots. As indicated in Chapter 1, coating cores with appropriate shells enhances the photoluminescence of the QDs. In this case the core is CdSe whose band gap is 1.7 eV is coated with ZnS whose band gap is 3.5 eV. Both materials, CdSe and ZnS, are known to be n-type intrinsic semiconductors and they can be synthesized with different sizes to cover the entire spectrum of the visible light.

Green CdSe / ZnS core-shell quantum dots were synthesized using the hot injection method previously reported in literature [50]. Four mmol of zinc acetate and 0.1 mmol of CdO were thoroughly mixed with 5 ml of oleic acid in a 50 ml flask. The temperature of the mixture was heated to 150 ^{o}C under degassing. When it reached to the desired temperature, 15 m of octadecene was injected in the flask and heated to 300 ^{o}C. At that temperature, another solution of 0.2 mmol of Se, 3 mmol of S, and 2 ml of trioctylphosphine was swiftly injected in the flask. The reaction lasted for 10 minutes, then the flask was cooled to room temperature to stop the reaction. The resulting quantum dots were purified four times using the centrifuge and by adding excess of methanol and hexane. Then, precipitated quantum dots were collected and dried under vacuum for 24 hours. The produced powder was dispersed in hexane to form an orange solution for further use in the deposition. Figure 2.4 (b) and (c) show the resulting QDs in solution under white light and UV light, respectively.

2.6 Molybdenum Trioxide Nanocrystals

Molybdenum trioxide is a wide band gap semiconductor with an n-type conductivity [51], [52] [53], [54]. Its n-type nature is attributed to the oxygen vacancies that work as electron donors to the conduction band [53], [54]. It has been widely used in the fabrication of solar cells and QD-LEDs as a hole extraction layer and a hole injection layer, respectively [53], [54]. In this work, MoO_3 nanoparticles were synthesized by following methods reported in literature [28]. A solution of 20 ml of oleylamine and 0.2 mmol of ammonium molybdate tetrahydrate were placed in a three neck flask under stirring for 30 minutes in order to degas the solution. Then, the temperature was raised to 100 ^oC and was kept at that temperature for 15 minutes before slowly raising it again to 250 ^oC. After three hours, the flask was allowed to cool to room temperature. Then the nanoparticles were purified by adding excess of acetone and using a centrifuge to separate the particles from the unwanted impurities. Finally, the precipitated particles were dried under vacuum for 24 hours before dispersing them in chloroform to be used in the device.

2.7 Device Fabrication

The structure of the fabricated device with the direction of the emitted light is illustrated in Figure 2.5. Two deposition techniques were followed in the fabrication of a QD-LED: spin coating, for the deposition of the device layers, and thermal evaporating for the metallization process. Commercial slides of indium tin oxide deposited on glass substrate were used as the anode of the device. Ultrasonic cleaning was used to clean the ITO slides with three solvents: deionized water, acetone, and isopropanol consecutively for 10 minutes for each. The prepared solution of nickel hydroxide was spin coated over the ITO substrate at 3000 rpm in a clean room,

and then the sample was annealed in a furnace for 15 minutes at 500 ^{o}C to produce a dark green thin film of nickel oxide.

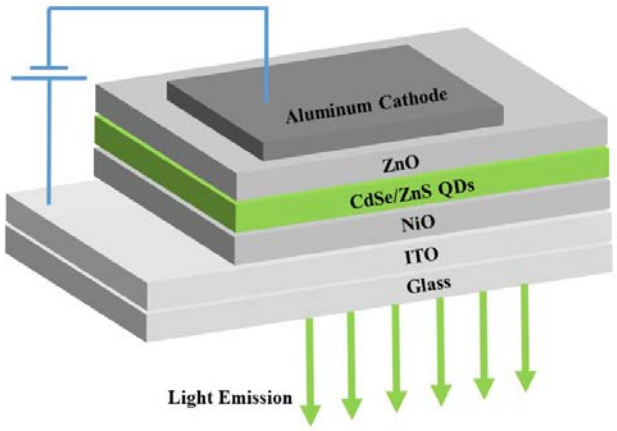

Figure 2.5: The complete structure of the fabricated QD-LED illustrating the bias voltage and the direction of the emitted light.

The second step of the fabrication was the deposition of the QDs, which was performed by spin coating the dispersed QDs over the nickel oxide thin film with 1000 rpm in a clean room. Then, the sample was annealed at 100 ^{o}C under nitrogen environment.

Zinc oxide nanocrystals dispersed in butanol were spin coated over the surface of the QD thin film at 2000 rpm. The annealing process was also performed in nitrogen environment at 110 ^{o}C. The last step of the fabrication was the metallization of the cathode. For this device, 100 nm of aluminum was deposited on the zinc oxide layer by using an Auto 306T Edwards thermal evaporator with a deposition rate as low as 1 nm per second to avoid a possible diffusion of the aluminum into the other layers and damaging the device.

Chapter 3 Characterization Methods

This chapter overviews the characterization techniques used to investigate the materials of this research and presents a summary of the theory of their working principles.

3.1 X-Ray Diffraction Spectroscopy

X-ray diffraction (XRD) spectroscopy is a non-destructive technique used to detect the crystallinity of an unknown material [55]. In this research, XRD was used to characterize the thin films of the nickel oxide. The basic principle of this technique is when an incident beam of x-rays hits a crystal, they interfere with each other as they move away from the crystal as shown in Figure 3.1.

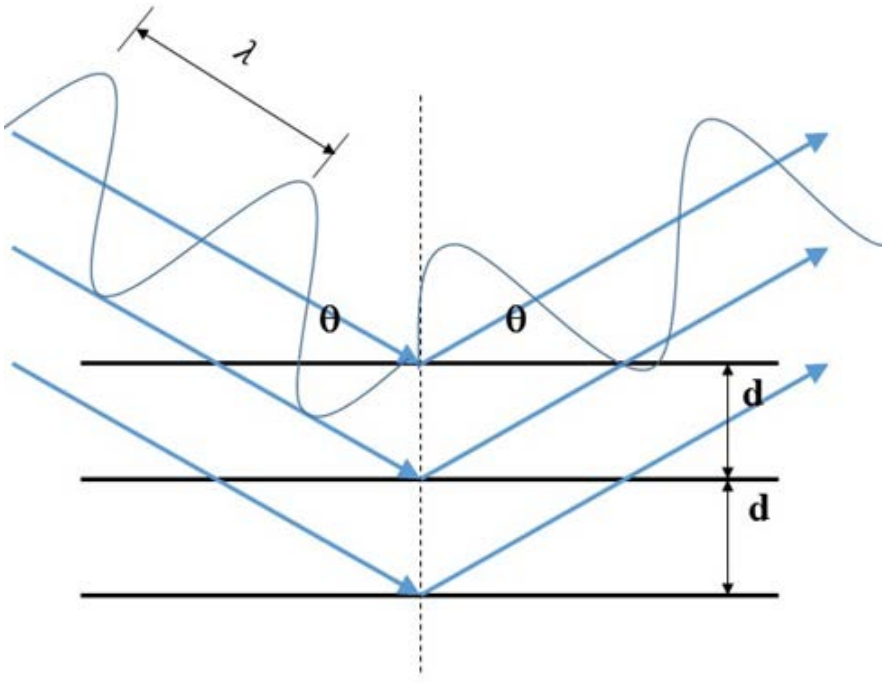

Figure 3.1: Schematic diagram illustrates the mechanism of XRD and Bragg's law.

The interference that takes place is constructive only when Bragg's law is satisfied as below:

$$n\lambda = 2d\ sin\theta \qquad \text{(Equation 3.1)}$$

where n is an integer number, λ is the wavelength of the incident light, d is the spacing between two planes in a crystal, and θ is the angle of the incident light. Thus, during the operation of this technique, the sample is rotated to cover a wide range of angles to detect the one that satisfies Bragg's law. The reason why X-ray waves are used in this technique is because the range of the spacing between planes is close to the wave length of X-rays.

Using the graph obtained by XRD spectroscopy, the crystallite size can be estimated using the following formula known as Scherrer Equation:

$$l = k\lambda/\beta cos\theta \qquad \text{(Equation 3.2)}$$

where l is the size of the grain, k is the shape factor, λ is the wavelength of the incident X-ray beam, β is the peak width measured at half of the maximum peak height , and θ is the angle of the X-ray beam.

Four important parameters are usually investigated when obtaining an XRD measurement. These parameters are location, intensity, shape, and width [56]. The location of the peak is simply a function of distance between the planes of the material as stated in Bragg's law. The peak shape on the other hand is not completely understood yet; it is reported that it is governed by Gaussian and Cauchy distributions, which results from two effects: coherent domain size and lattice strain, respectively [56]. The width of the peak is inversely proportional to the size of the grain according to Scherrer Equation. In this research, Scherrer equation was used to estimate the grain size of the NiO thin film deposited on glass.

3.2 Absorption Spectroscopy

A Cary 500 UV-Vis spectrophotometer was used to obtain the absorbance spectrum of ZnO nanocrystals and CdSe-ZnS core-shell quantum dots. Absorption spectroscopy is a technique that provides the absorption spectrum as a function of wavelength. In this technique, a range of wavelengths hits the sample and the output waves are detected to measure how much absorption the reflected waves were subjected to [57].

The main parts of a typical absorbance spectroscopy are shown in Fig. 3-2 (a). The amount of absorption is different at each wavelength and it is an indicator of the inter-band transitions that take place when the electromagnetic waves are absorbed. The latter process is the transition of an electron from the valance band to the conduction band when it is excited by a photon [57], [58].

As a condition for the transition to take place, the photon energy should be equal or higher than the energy difference between the valance band and the conduction band. Thus, absorbance spectroscopy is a method to extract the band gap of a material. The following equation is Beer's law, which is the simplest representation of the absorbance mechanism:

$$I(z) = I^{\circ} \exp[-\alpha(\omega)z] \qquad \text{(Equation 3.3)}$$

where $I(z)$ and I° are the intensities of the electromagnetic wave at a distance z inside the sample and at the surface of the sample respectively, and $\alpha(\omega)$ is the absorption coefficient of the sample. Figure 3.2 (b) shows the Cary 500 UV-Vis spectrophotometer used to characterize the ZnO NCs and the QDs in solution. The experiment was set up as follows: the baseline of the spectrum was measured by using the cuvette full of butanol for the ZnO measurements and chloroform for the QDs measurements. Then, the range of frequencies was set from 200 nm to 800 nm to obtain the absorbance spectrum.

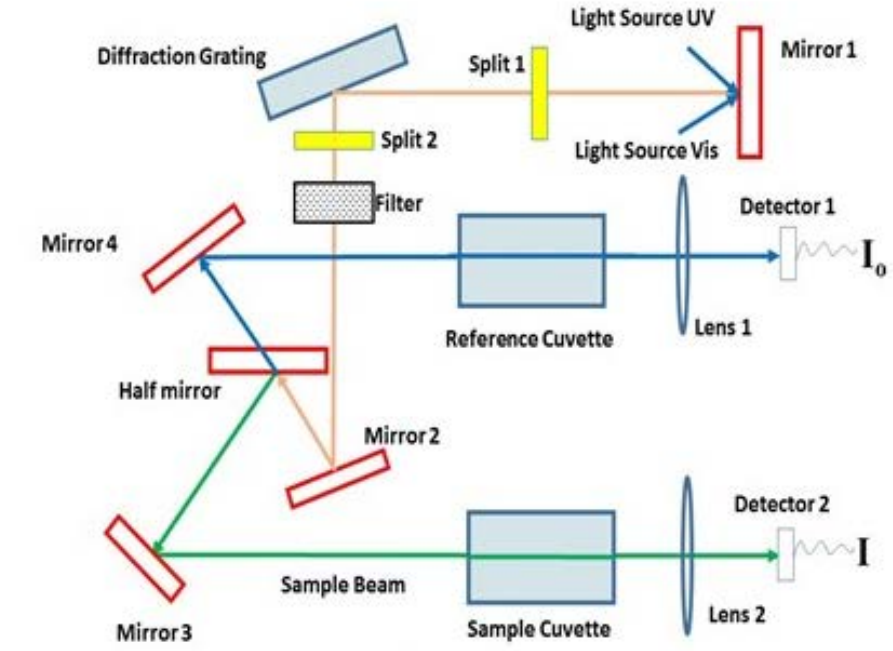

(a)

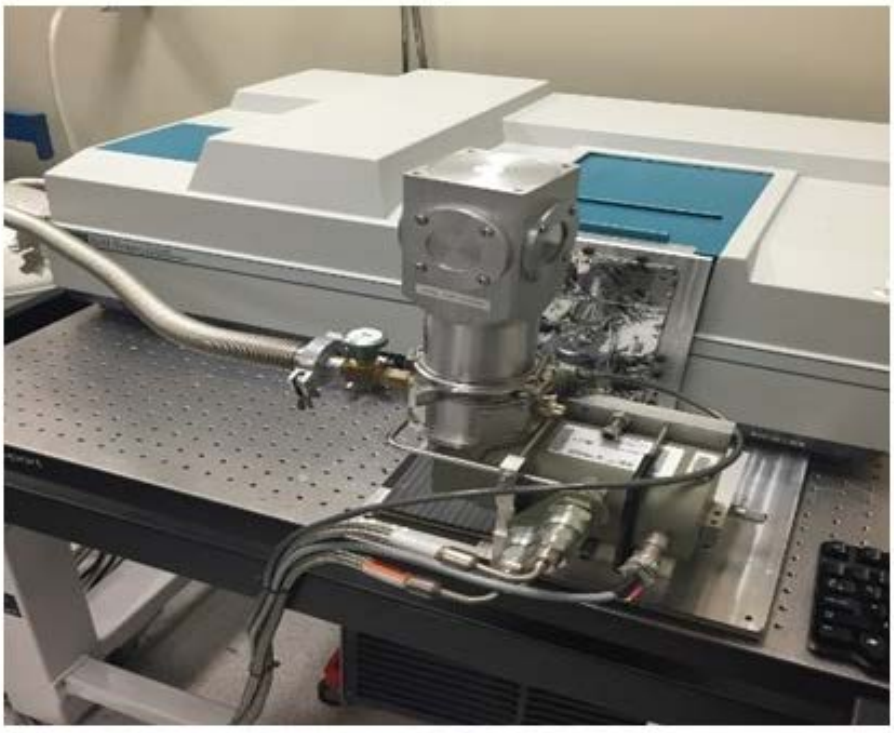

(b)

Figure 3.2 (a) Schematic diagram illustrating the working principle of the absorbance spectroscopy. (b) Carry 500 UV absorbance spectrometer.

3.3 Photoluminescence Spectroscopy

Photoluminescence spectroscopy was used to observe the emission behavior of the ZnO nanocrystals and the quantum dots deposited on glass substrates. Generally, photoluminescence spectroscopy identifies the emission spectrum of an unknown material, giving insight about strain, doping, damage inside the crystal, microscopic defects, and thickness [58]. Photoluminescence is a process by which an electron decays from the conduction band to the valence band and emits a photon [58]. The working principle of this technique is that a sample is hit by a laser beam, which excites the electrons of the samples before they decay back producing photoluminescence. Figure 3.3 shows a basic schematic diagram of the PL spectrometer and a photo of the one used in this research. To obtain the PL spectrum of the ZnO and the QDs, thin films of both materials deposited on glass substrates were used. To obtain a better quality spectrum, it is preferred to have a multilayer thin film to increase the thickness.

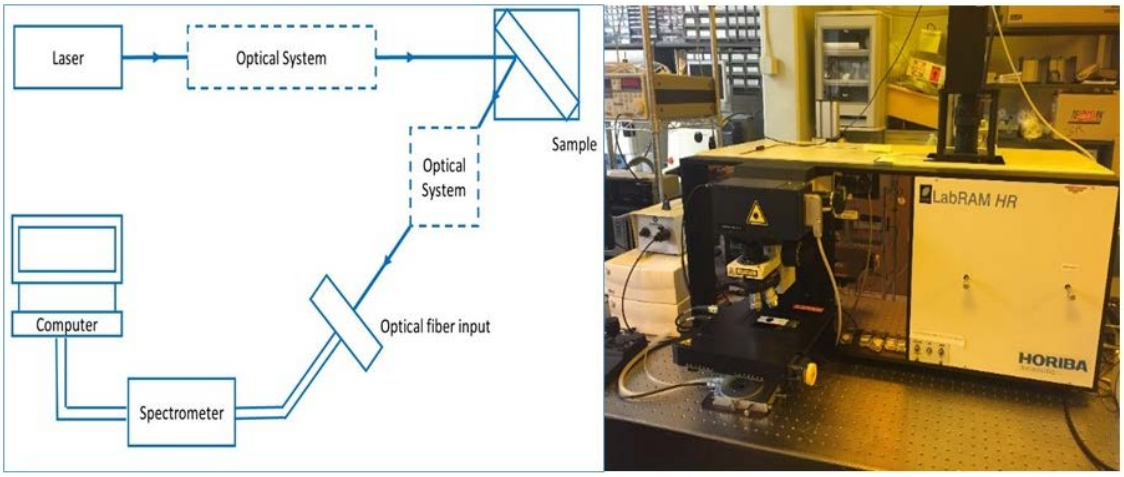

Figure 3.3: (a) Schematic diagram illustrating the working principles of the micro-photoluminescence spectroscopy. (b) Micro-photoluminescence spectrometer used in this research.

3.4 Raman Spectroscopy

Raman spectroscopy depends on the inelastic scattering of light when it interacts with the atoms of the sample. The obtained data are the intensity of light, which is a measurement of the number of photons versus the frequency shift. The latter quantity is the difference between the frequency of the light source and that of the scattered light [44], [57]. When the frequency of the scattered light is more than the original frequency, the process is called Stokes-Raman shift. The anti-Stokes-Raman shift occurs when the scattered frequency is higher than the original frequency [44], [57]. Phonons (lattice vibrations) are mainly the reason behind this elastic scattering, by which Raman spectrum can provide information about the chemical composition and crystalline structure. Raman spectrum depends on the following equation:

$$p = \alpha E \qquad \text{(Equation 3.4)}$$

where p is the induced electrical dipole moment when the light hits the sample, E is the electric field, and α is the polarizability of the material. The latter quantity is a measurement of how easy an external electric field can interrupt the electron distribution.

Equation (3.4) is expanded to the following formula that contains the three types of scattering [57]:

$$p = \alpha E \cos(2\pi vin) + \frac{\partial \alpha}{\partial Q}\frac{QE}{2}[\ \cos 2\pi t(vin - vbin) + cos2\pi t(vin + vbin)] \qquad \text{(Equation 3.5)}$$

where $\alpha E \cos(2\pi vin)$ is related to Raleigh scattering at which no change in energy takes place. $\cos 2\pi t(vin - vbin)$ is related to Stokes-Raman scattering at which the output frequency is less than the input frequency, and $\cos 2\pi t(vin + vbin)$ is related to the anti-Stokes-Raman shift, where the output frequency is more than the input frequency [57]. The positions of these shifts prove whether a certain material exists. For this research, Raman spectrum was obtained for the

ZnO NCs and MoO_3 using the same instrument in Figure 3.3 (b) which can be used to obtain both Raman and PL spectra.

3.5 Atomic Force Microscopy

Atomic force microscopy (AFM) is one of the techniques that are used to provide high resolution images of a surface. In this work, AFM was used to obtain an image of the NiO thin film surface as well as the RMS value of the surface roughness [57]. The working principle of this technique is depicted in Figure 3.4.

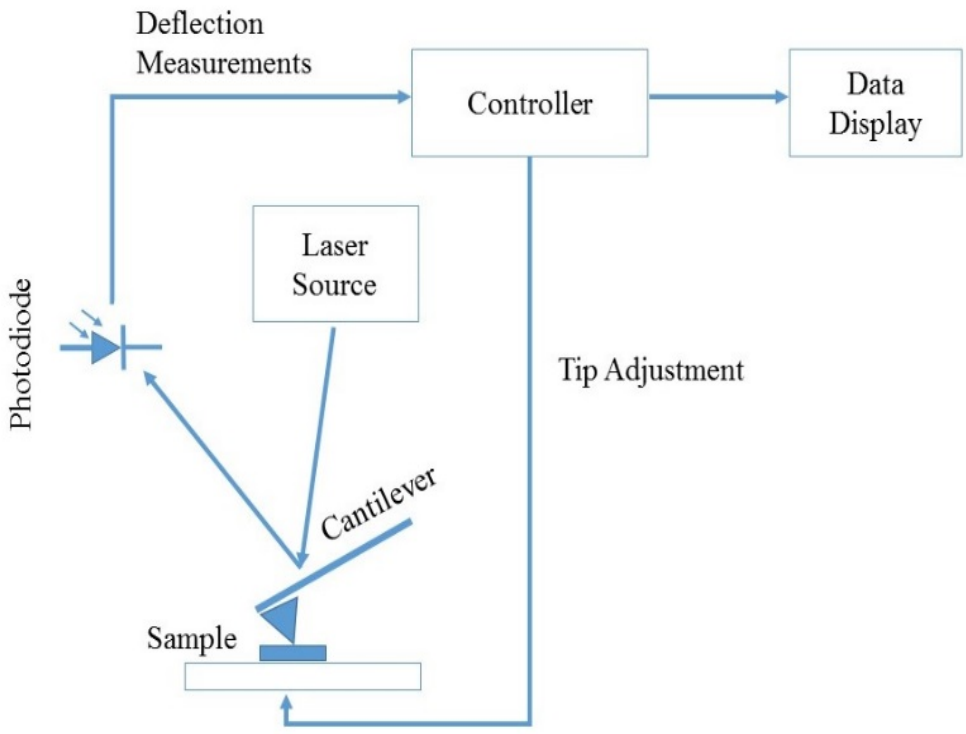

Figure 3.4: Schematic diagram illustrating the working principles and the main parts of the atomic force microscope.

During the measurements, the tip of the cantilever scans the surface of the sample. When the tip is few nanometers from the surface of the sample, the effect of Van Der Waals forces, electrostatic forces, and several other surface forces starts to appear. The effect of these forces deflects the tip of the cantilever, which diverts the reflected laser beam. The controller adjusts the position of the cantilever based on the feedback of the reflected laser beam. This technique provides a surface image of a sample with a high resolution (as high as hundreds of picometers) [57].

Chapter 4 Results and Discussion

4.1 X-ray Diffraction Measurements

The crystallinity of the nickel oxide thin films was investigated using XRD spectroscopy as illustrated in Figure 4.1. The results exhibited a polycrystalline material with three diffraction peaks located at the angles 37º, 43º, and 64º which were related the planes (111), (200), and (220). By using the Scherrer equation for the first peak, an estimation of the NiO grain size was found to be 12 nm.

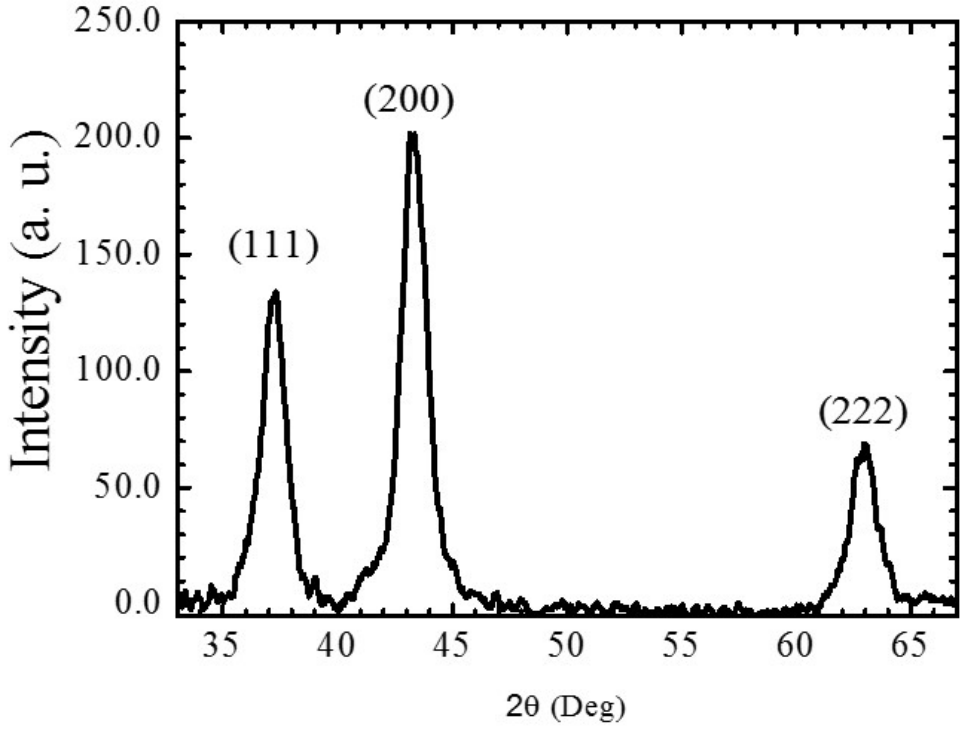

Figure 4.1: X-ray diffraction measurements of nickel oxide thin film exhibit three peaks at the angles 37º, 43º, and 64º.

4.2 Nickel Oxide Surface Imaging

The surface morphology of the NiO thin film was evaluated by obtaining AFM images as shown in Figure 4.2. It was found that the RMS roughness value of 1x1 mm surface area of NiO

thin film deposited on an ITO slide was 2 nm. This value was mainly attributed to the ITO substrate and the poor capability of the NiO to passivate this roughness. Lower values of roughness are reported for glass and fluorine doped tin oxide (FTO) substrates.

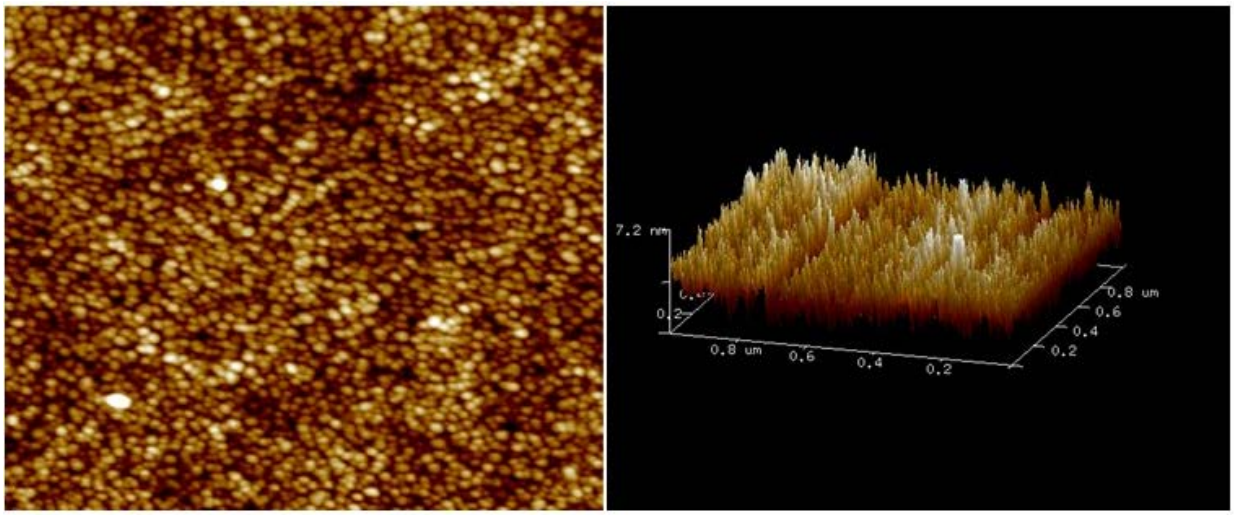

Figure 4.2: 2D and 3D images of 1x1 mm surface area of nickel oxide thin film obtained by atomic force microscopy.

4.3 Absorbance and Photoluminescence Measurements

Figure 4.3 illustrates the absorbance and photoluminescence spectrum of ZnO nanocrystals. The threshold of the optical absorbance spectrum was located at 355 nm while the emission peak was located at 370 nm. Both peaks were related to the value of the material band gap, thus they should have had the same value at the same temperature. The reason behind the difference of the two values was the energy released to the lattice by the electron-phonon coupling [57]. In general, the absorption energy is higher than the emission energy by a factor called the Stokes shift which is an indicator of the electron-phonon coupling strength.

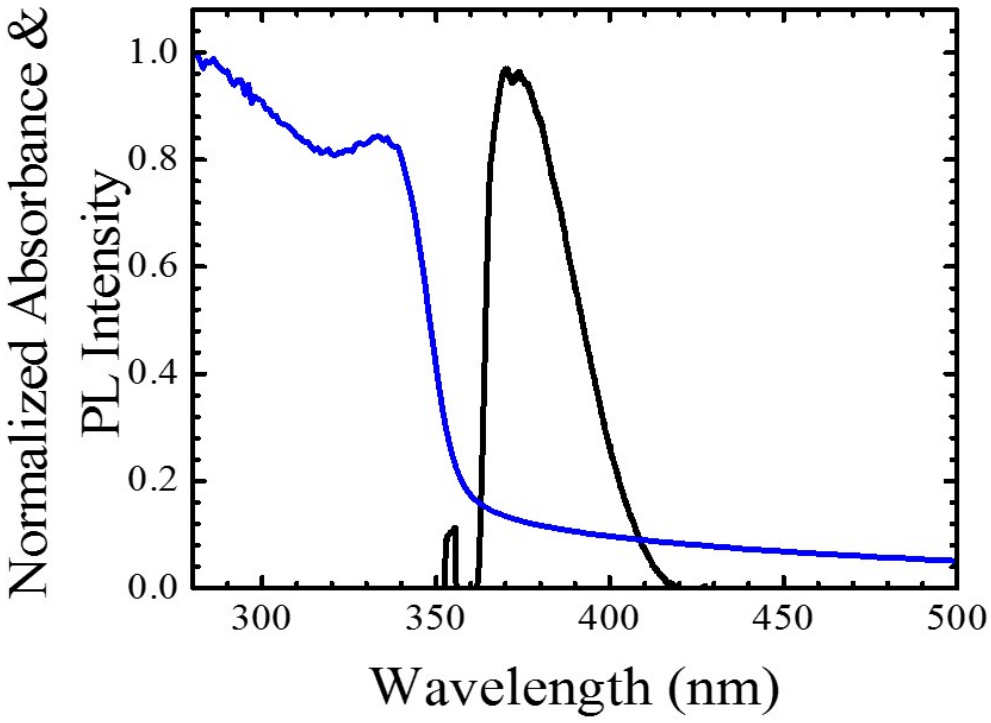

Figure 4.3: Micro-photoluminescence and absorbance spectra of zinc oxide nanocrystals deposited on glass substrate. The emission peak was observed at 370 nm of the PL spectrum, while the absorbance spectrum has a threshold value at 355 nm.

The same measurements were taken for the CdSe/ZnS QDs as shown in Figure 4.4. An emission peak was located at 515 nm indicating a green color and, similar to what was observed in the previous figure, the energies of the absorption spectrum were higher than that of the emission spectrum. The FWHM of the QD PL spectrum was around 45 nm which reflected a fair amount of QD size variation. Although it was clear that FWHM is an interpretation of the size variation, up to now, there is no direct method to numerically extract the percentage of the size variation from the PL spectrum.

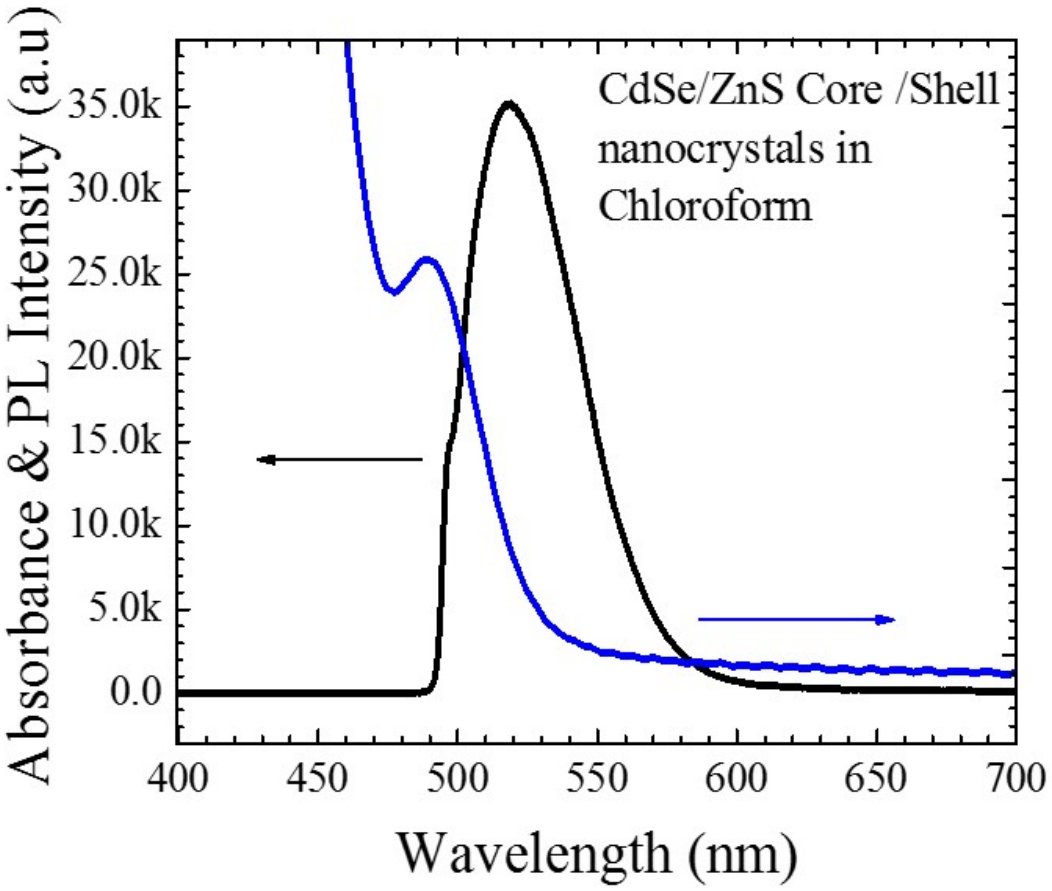

Figure 4.4: Micro-photoluminescence and absorbance spectrum of CdSe / ZnS core-shell quantum dots. The emission peak is located at 515 with a FWHM of 45 nm

4.4 Raman shifts

Thin flim ZnO NCs deposited on a glass substrate were used to obtain the Raman spectrum. ZnO usually takes the form of wurtzite crystal structure, which means it has 4 atoms in a unit cell and 12 phonon modes. Three of these phonon modes are acoustic and the rest are optical [44]. Among those phonons, E_2 high which is one of the phonon modes for this material

which has the sharpest peak located at 440 cm $^{-1}$ and is related to the vibration of the oxygen atom as shown in Figure 4.5.

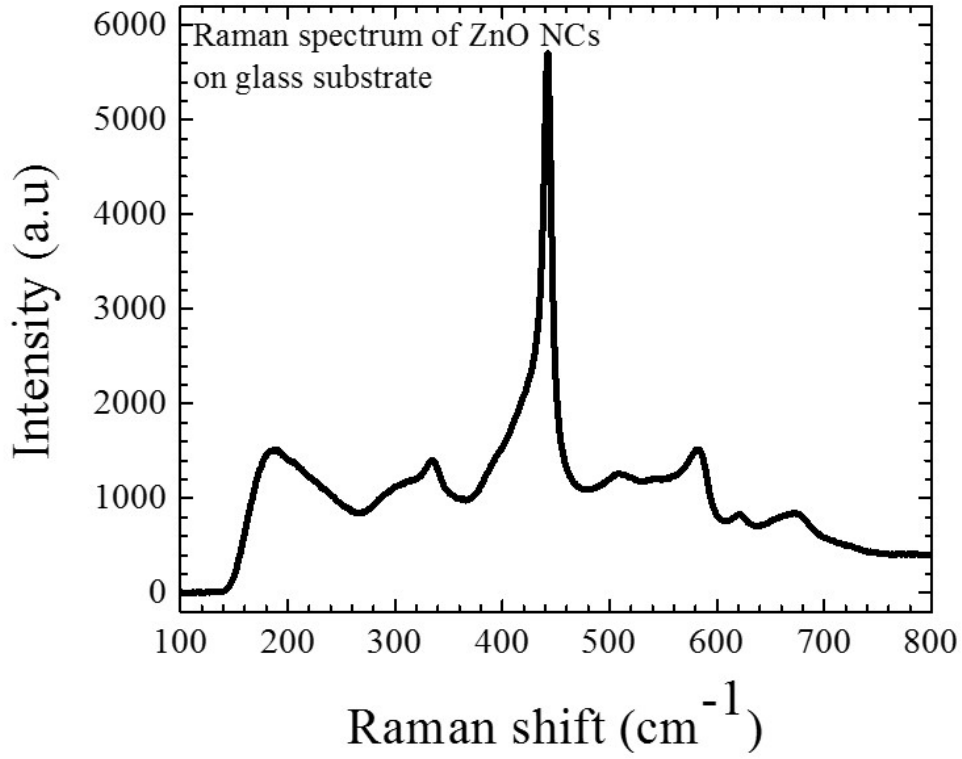

Figure 4.5: Raman spectrum of zinc oxide NCs thin film with a center peak at 440 cm $^{-1}$ and two adjacent peaks at 320 cm^{-1} and 580 cm^{-1}.

The peak located at 320 cm^{-1} was related to the second-order Raman scattering of E_2-E_1, which was the result of the interaction between the two mentioned phonons [58]. Unlike bulk ZnO, the Raman spectrum of ZnO nanostructure didn't exhibit TO phonons as confirmed by these measurements [59]. On the other hand, a peak was observed at 580 cm^{-1}, which was related to the A_1 LO mode that is only seen in ZnO nanostructure material [59].

Molybdenum trioxide was characterized using Raman spectroscopy. For this purpose, a thin film of MoO_3 deposited on a glass substrate was used as a sample. The obtained results coincided with what is reported in literature for MoO_3 [14],[60]. Six peaks were observed at 270,

330, 370, 660, 820 and 990 cm^{-1} as shown in Figure 4.6. It is reported that the peaks located in the region 900 cm^{-1} to 600 cm^{-1} originate from the stretching mode of Mo-O while the bending mode results in the shifts located in the region 400 cm^{-1} to 200 cm^{-1}.

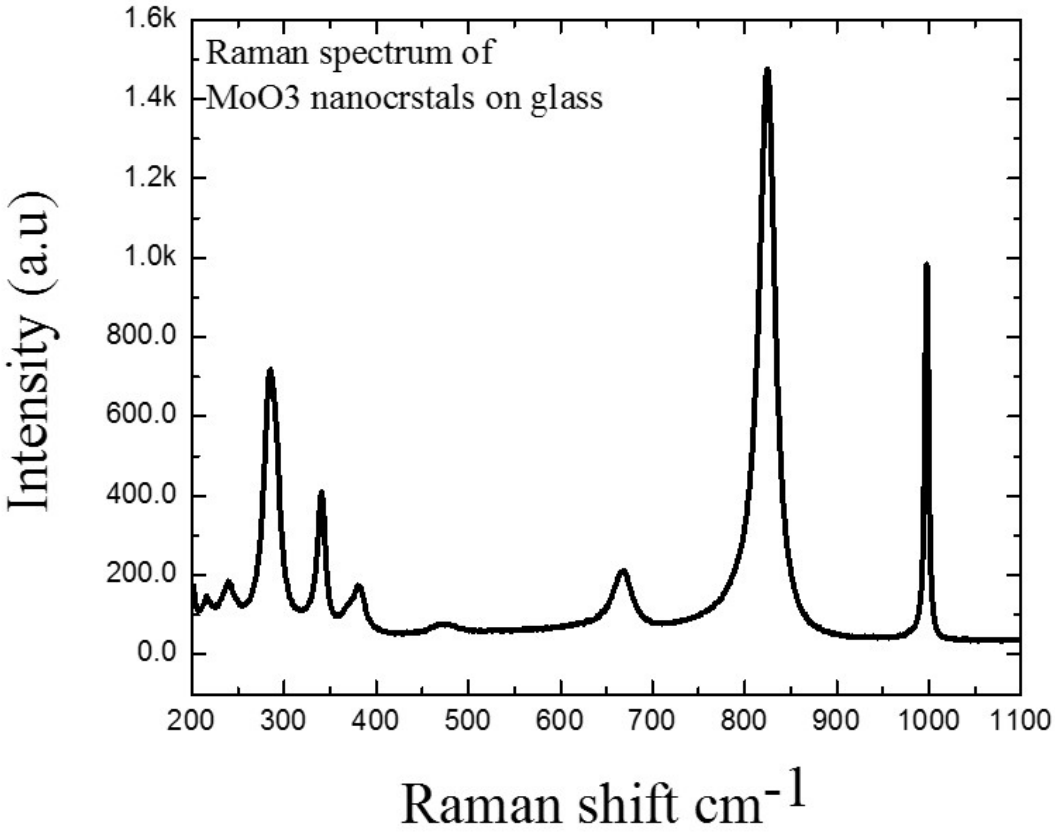

Figure 4.6: Raman spectrum of molybdenum trioxide nanocrystals deposited on glass substrate exhibits nine sharp peaks.

4.5 Quantum Dots LED Current Voltage Characteristics

The transfer characteristics curve was obtained using a Keithley SCS 4200 semiconductor characterization. The range of the input voltage was set from 0 to 9 V. An important feature of the device is the turn on voltage, which is the value of the bias voltage at

which the device starts to operate and produce clear light. So far, the reported values of the QD-LEDs turn on voltage are still high which is one of the challenges that needs to be addressed in the future. As illustrated in Figure 4.7, it is hard to identify one single point as the turn on voltage, but it can be observed that there was no current with a voltage less than 3 V and it started to ramp up after 5 V. The inset images show the device with and without bias voltage with pure green light. At 9 V, the value of the current density was 160 mA cm^{-2}.

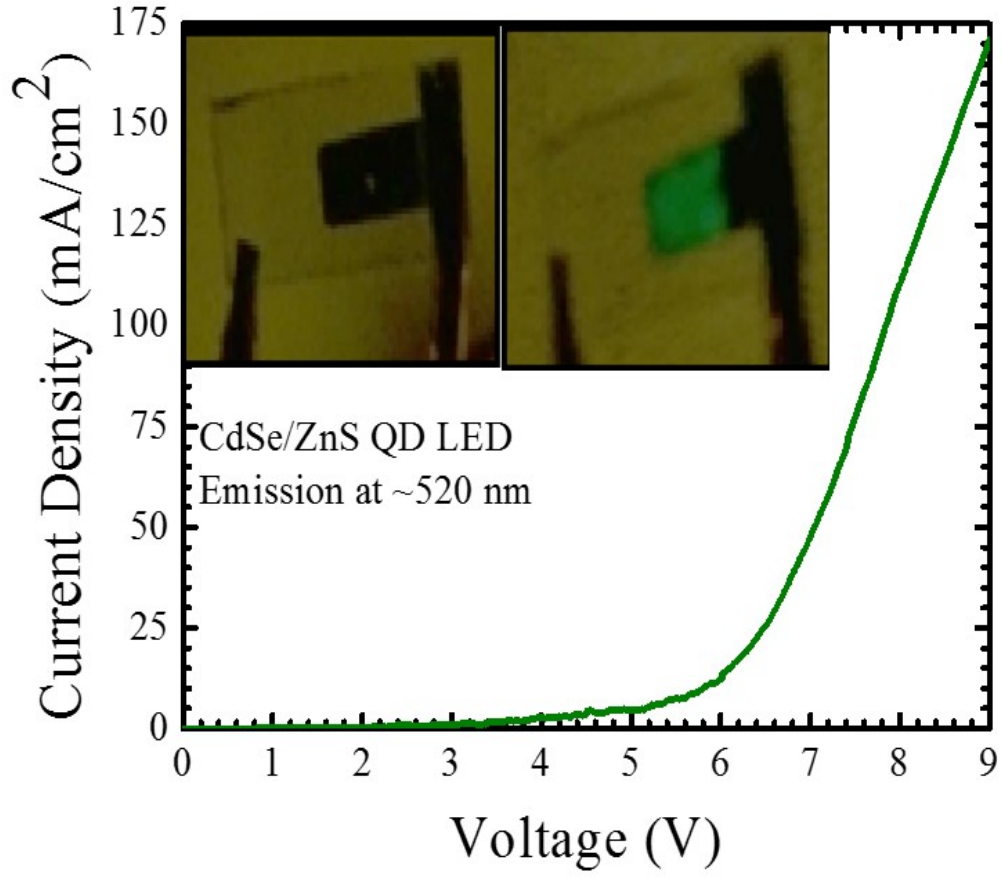

Figure 4.7: Current voltage characteristic curve of the fabricated quantum dots LED.

Chapter 5 Summary and Future Work

5.1 Summary of the Conducted Research

To summarize the work of this thesis, four inorganic materials were synthesized using methods reported in literature. These methods were modified as necessary. The synthesized materials were NiO, ZnO, CdSe/ ZnS QDs, and MoO_3 which were chosen because of their low cost and optimized synthesis procedure. Five characterization techniques were used to test the materials and to make sure they had a proper quality that was sufficient to fabricate a device. The deposition of the device layers was performed using a spin-coting technique also because of its low cost. For the purpose of metallization, Auto 306T Edwards thermal evaporator was used to deposit 100 nm of aluminum. All the results obtained for this thesis in terms of material characterization and the device characteristics were consistent with data in literature.

5.2 Future Work

As mentioned previously, the whole mechanism and the working principle of this device is not well understood, so there is still much work to do to understand the theoretical principles behind it. Up to now, the efficiency of all inorganic LEDs is less than 1%, which means it needs much improvement before they can be practically used in lighting applications. Part of this improvement requires a clear understanding of the role of Auger recombination which is believed to have a big part of the non-radiative recombination. Another problem that needs to be addressed is the increasing number of the charged QDs when the device operates under high values of current. This problem confines the usage of these devices to only low current applications. Studying other materials as hole and electron transport layers will open the door for more efficient devices. The balance between the injection rate of the holes and electrons is a key factor to having a more efficient device. However, most of the materials studied so far

produce a high barrier for the holes compared with the barrier for electrons; new materials might overcome this problem. Finally, obtaining lower turn on voltage for these devices has also been a focus of researchers and it mainly depends on the band alignment of the device, i.e. the barriers of transport layers and the QD band gap.

References

[1] Konstantatos, G., and Sargent, E. H. (2013). Colloidal quantum dot optoelectronics and photovoltaics. 61-95. http://doi.org/http://dx.doi.org/10.1017/CBO9781139022750

[2] Talapin, D. V., and Steckel, J. (2013). Quantum dot light-emitting devices. *MRS Bulletin*, *38*(09), 685–691. http://doi.org/10.1557/mrs.2013.204

[3] Talapin, D. V, Lee, J., Kovalenko, M. V, and Shevchenko, E. V. (2010). Prospects of Colloidal Nanocrystals for Electronic and Optoelectronic Applications, Chem. Review, 389–458.

[4] Shirasaki, Y., Supran, G. J., Bawendi, M. G., and Bulović, V. (2013). *Nature Photonics*, *7*(12), 933–933. http://doi.org/10.1038/nphoton.2013.328

[5] Supran, G.J., Shirasaki, Y., Song, K.W., Caruge, J.-M., Kazlas, P.T., Coe-Sullivan, S., Andrew, T.L., Bawendi, M.G. and Bulović, V. (2013) QLEDs for displays and solid-state lighting', *MRS Bulletin*, 38(9), pp. 703–711. doi: 10.1557/mrs.2013.181

[6] Bae, W.K., Brovelli, S. and Klimov, V.I. (2013) Spectroscopic insights into the performance of quantum dot light-emitting diodes, *MRS Bulletin*, 38(9), pp. 721–730. doi: 10.1557/mrs.2013.182.

[7] Bozyigit, D. and Wood, V. (2013) Challenges and solutions for high-efficiency quantum dot-based LEDs, *MRS Bulletin*, 38(9), pp. 731–736. doi: 10.1557/mrs.2013.180.

[8] Cao, G., and Wang, Y. (2004). Nanostructure & Nanomaterial: Synthesis, properties & applications. Imperial College Press. 15-89.

[9] Chen, O., Wei, H., Maurice, A., Bawendi, M. and Reiss, P. (2013) Pure colors from core–shell quantum dots, *MRS Bulletin*, 38(9), pp. 696–702. doi: 10.1557/mrs.2013.179.

[10] Stavrou, V.N. (2015). Quantum Dots Theory and Applications. AvE4EvA. 34-71. http://doi.org/10.5772/59735

[11] Kim, S. S.-W., Im, S. H., and Kim, S. S.-W. (2013). Performance of light-emitting-diode based on quantum dots. *Nanoscale*, *5*(12), 5205–14. http://doi.org/10.1039/c3nr00496a

[12] Reiss, P., Protière, M., and Li, L. (2009). Core/Shell Semiconductor Nanocrystals. *Small*, *5*(2), 154–168. http://doi.org/10.1002/smll.200800841

[13] Kim, S., Fisher, B., and Bawendi, M. (2003). Type-II Quantum Dots : CdTe / CdSe (Core / Shell) and CdSe / ZnTe (Core / Shell) Heterostructures, ACS.11466–11467.

[14] Rabindar K Sharma and G. B. Reddy. (2014). Synthesis and characterization of - MoO_3 microspheres packed with nanoflakes. IOP Science, 4(6), 3. 065305 http://doi.org10.1088/0022-3727/47/6/065305

[15] M. Dieterle and G. Mestl. (2001). Part II.y Resonance Raman spectroscopic characterization of the molybdenum oxides Mo4O11 and MoO2. Phys. Chem. 822-826. http://doi.org/10.1038/285176a0

[16] Deng, Z., and Guyot-sionnest, ACS Nano, P. 2121–2127. (2016). Intraband Luminescence from HgSe/CdS Core/ Shell Quantum Dots. http://doi.org/10.1021/acsnano.5b06527

[17] Pal, B. N., Ghosh, Y., Brovelli, S., Laocharoensuk, R., Klimov, V. I., Hollingsworth, J., and Htoon, H. (2012). "Giant" CdSe/CdS core/shell nanocrystal quantum dots as efficient electroluminescent materials: Strong influence of shell thickness on light-emitting diode performance. *Nano Letters*, *12*(1), 331–336. http://doi.org/10.1021/nl203620f

[18] Gong, K., and Kelley, D. F. (2015). Lattice Strain Limit for Uniform Shell Deposition in Zincblende CdSe/CdS Quantum Dots. *The Journal of Physical Chemistry Letters*, 1559–1562. http://doi.org/10.1021/acs.jpclett.5b00566

[19] Yang, Y., Zheng, Y., Cao, W., Titov, A., Hyvonen, J., Manders, J. R. Qian, L. (2015). High-efficiency light-emitting devices based on quantum dots with tailored nanostructures. *Nature Photonics*, *9*(March), 1–9. http://doi.org/10.1038/nphoton.2015.36

[20] Smith, A. M., Mohs, A. M., and Nie, S. (2008). Tuning the optical and electronic properties of colloidal nanocrystals by lattice strain. *Nature Nanotechnology*, *4*(1), 56–63. http://doi.org/10.1038/nnano.2008.360

[21] Bozyigit, D., Yarema, O., and Wood, V. (2013). Origins of low quantum efficiencies in quantum dot LEDs. *Advanced Functional Materials*, *23*(24), 3024–3029. http://doi.org/10.1002/adfm.201203191

[22] Noginov, M. A. . (2009). Tutorials in Complex Photonic Media. *Journal of Oral Science*, *46*, 696. http://doi.org/10.1117/3.832717

[23] Dang, C. and Nurmikko, A. (2013) Beyond quantum dot LEDs: Optical gain and laser action in red, green, and blue colors', *MRS Bulletin*, 38(9), pp. 737–742. doi: 10.1557/mrs.2013.183.

[24] Ji, W., Jing, P., Zhang, L., Li, D., Zeng, Q., Qu, S., and Zhao, J. (2014). The work mechanism and sub-bandgap-voltage electroluminescence in inverted quantum dot light-emitting diodes. *Scientific Reports*, *4*(1), 6974. http://doi.org/10.1038/srep06974

[25] Supran, G. J., Shirasaki, Y., Song, K. W., Caruge, J.-M., Kazlas, P. T., Coe-Sullivan, S., Bulović, V. (2013). QLEDs for displays and solid-state lighting. *MRS Bulletin*, *38*(09), 703–711. http://doi.org/10.1557/mrs.2013.181

[26] Bae, W. K., Park, Y.-S., Lim, J., Lee, D., Padilha, L. A., McDaniel, H.,Klimov, V. I. (2013). Controlling the influence of Auger recombination on the performance of quantum-dot light-emitting diodes. *Nature Communications*, *4*, 1–8. http://doi.org/10.1038/ncomms3661

[27] Garcia-Santamaria, F., Chen, Y., Vela, J., Hollingsworth, J. A., Schaller, R. D., and Klimov, V. I. (2009). Suppressed Auger Recombination in Giant Nanocrystals Boosts Optical Gain Performance. *Nano Lett.*, *9*(10), 3482–3488. http://doi.org/10.1021/nl901681d

[28] Bhaumik, S., and Pal, A. J. (2014). Light-emitting diodes based on solution-processed nontoxic quantum dots: oxides as carrier-transport layers and introducing molybdenum oxide nanoparticles as a hole-inject layer. *ACS Applied Materials & Interfaces*, *6*(14), 11348–56. http://doi.org/10.1021/am501890m

[29] Kwak, J., Bae, W. K., Lee, D., Park, I., Lim, J., Park, M., Lee, C. (2012). Bright and efficient full-color colloidal quantum dot light-emitting diodes using an inverted device structure. *Nano Letters*, *12*(5), 2362–2366. http://doi.org/10.1021/nl3003254

[30] Attia, S., Wang, J., Wu, G., Shen, J., and Ma, J. (2002). Review on Sol—Gel Derived Coatings: Process, Techniques and Optical Applications. *Journal of Materials Science & Technology*. Retrieved from http://www.cqvip.com/qk/84252x/200203/6982802.html

[31] Danks, A. E., Hall, S. R., and Schnepp, Z. (2016). Materials horizons technique for materials synthesis. *Materials Horizons*, *3*, 91–112. http://doi.org/10.1039/C5MH00260E

[32] Donegμ, C. D. M., Liljeroth, P., and Vanmaekelbergh, D. (2005). Physicochemical Evaluation of the Hot-Injection Method, a Synthesis Route for Monodisperse Nanocrystals, Wiley, (12), 1152–1162. http://doi.org/10.1002/smll.200500239

[33] Mashford, B. S., Nguyen, T.-L., Wilson, G. J., and Mulvaney, P. (2010). All-inorganic quantum-dot light-emitting devices formed via low-cost, wet-chemical processing. *Journal of Materials Chemistry*, *20*(1), 167. http://doi.org/10.1039/b905256a

[34] Lemire, H. M., Peterson, K. a., Sprawls, S., Singer, K., Martin, I. T., and French, R. H. (2013). Degradation of transparent conductive oxides: mechanistic insights across configurations and exposures. *Proceedings of SPIE*, 882502. http://doi.org/10.1117/12.2024691

[35] Friedel, B., Brenner, T. J. K., McNeill, C. R., Steiner, U., and Greenham, N. C. (2011). Influence of solution heating on the properties of PEDOT:PSS colloidal solutions and impact on the device performance of polymer solar cells. *Organic Electronics: Physics, Materials, Applications*, *12*(10), 1736–1745. http://doi.org/10.1016/j.orgel.2011.07.003

[36] Zhou, J., Anjum, D. H., Chen, L., Xu, X., Ventura, I. A., Jiang, L., and Lubineau, G. (2014). The temperature-dependent microstructure of PEDOT/PSS films: insights from morphological, mechanical and electrical analyses. *J. Mater. Chem. C*, *2*(46), 9903–9910. http://doi.org/10.1039/C4TC01593B

[37] Steirer, K. X., Chesin, J. P., Widjonarko, N. E., Berry, J. J., Miedaner, A., Ginley, D. S., and Olson, D. C. (2010). Solution deposited NiO thin-films as hole transport layers in organic photovoltaics. *Organic Electronics*, *11*(8), 1414–1418. http://doi.org/10.1016/j.orgel.2010.05.008

[38] Caruge, J. M., Halpert, J. E., Bulović, V., and Bawendi, M. G. (2006). NiO as an inorganic hole-transporting layer in quantum-dot light-emitting devices. *Nano Letters*, *6*(12), 2991–2994. http://doi.org/10.1021/nl0623208

[39] Jlassi, M., Sta, I., Hajji, M., Haoua, B. Ben, and Ezzaouia, H. (2014). Effect of annealing atmosphere on the electrical properties of nickel oxide/zinc oxide p–n junction grown by sol–gel technique. *Materials Science in Semiconductor Processing*, *26*, 395–403. http://doi.org/10.1016/j.mssp.2014.05.008

[40] Manders, J. R., Tsang, S.-W., Hartel, M. J., Lai, T.-H., Chen, S., Amb, C. M., So, F. (2013). Solution-Processed Nickel Oxide Hole Transport Layers in High Efficiency Polymer Photovoltaic Cells. *Advanced Functional Materials*, *23*(23), 2993–3001. http://doi.org/10.1002/adfm.201202269

[41] Jiang, F., Choy, W. C. H., Li, X., Zhang, D., and Cheng, J. (2015). Post-treatment-Free Solution-Processed Non-stoichiometric NiO $_x$ Nanoparticles for Efficient Hole-Transport Layers of Organic Optoelectronic Devices. *Advanced Materials*, *27*(18), 2930–2937. http://doi.org/10.1002/adma.201405391

[42] Liu, S., Liu, R., Chen, Y., Ho, S., Kim, J. H., and So, F. (2014). Nickel oxide hole injection/transport layers for efficient solution-processed organic light-emitting diodes. *Chemistry of Materials*, *26*(15), 4528–4534. http://doi.org/10.1021/cm501898y

[43] Janotti, A., Van de Walle, C. G., and Walle, C. G. Van De. (2009). Fundamentals of zinc oxide as a semiconductor. *Reports on Progress in Physics*, *72*(12), 126501. http://doi.org/10.1088/0034-4885/72/12/126501

[44] Schumm, M. (2008). ZnO-based semiconductors studied by Raman spectroscopy : semimagnetic alloying, doping, and nanostructures. Dissertation, university of Wurzburg, 36-71.

[45] Lv, Y., Xiao, W., Li, W., Xue, J., and Ding, J. (2013). Controllable synthesis of ZnO nanoparticles with high intensity visible photoemission and investigation of its mechanism. *Nanotechnology*, *24*(17), 175702. http://doi.org/10.1088/0957-4484/24/17/175702

[46] Mang, A. (1995). Reimann, and St. Riibenacke, *Elsevier*, *94*(4), 251–254. http://doi.org/10.1016/0038-1098(95)00054-2

[47] Janotti, A., Walle, C. G. Van De, Janotti, A., and Walle, C. G. Van De. (2014). Oxygen vacancies in ZnO Oxygen vacancies in ZnO, *Applied Physics*, *122102*(2005). http://doi.org/10.1063/1.2053360

[48] A. J., and Walle, C. G. Van De. (2006). New insights into the role of native point defects in ZnO, *287*, 58–65. http://doi.org/10.1016/j.jcrysgro.2005.10.043

[49] Janotti, A., & Walle, C. G. Van De. (2007). Native point defects in ZnO, (April), 1–22. http://doi.org/10.1103/PhysRevB.76.165202

[50] Ki Bae, W., Kwak, J., Park, J. W., Char, K., Lee, C., and Lee, S. (2009). Highly Efficient Green-Light-Emitting Diodes Based on CdSe@ZnS Quantum Dots with a Chemical-Composition Gradient. *Advanced Materials*, *21*(17), 1690–1694. http://doi.org/10.1002/adma.200801908

[51] Kröger, M., Hamwi, S., Meyer, J., Riedl, T., Kowalsky, W., Kahn, A, Kahn, A. (2015). Role of the deep-lying electronic states of MoO 3 in the enhancement of hole- injection in organic thin films Role of the deep-lying electronic states of MoO 3 in the enhancement of hole-injection in organic thin films, *123301*(2009), 4–7. http://doi.org/10.1063/1.3231928

[52] Talik, N. A., Woon, K. L., Yap, B. K., Wong, W. S., Whitcher, T. J., Chanlek, N., Songsiriritthigul, P. (n.d.). layers Highly efficient processable molybdenum trioxide as a hole blocking interlayer for super-yellow organic light emitting diode. *Journal of Physics D: Applied Physics*, 395105. http://doi.org/10.1088/0022-3727/49/39/395105

[53] Buono-Core, G. E., Klahn, A. H., Castillo, C., Muñoz, E., Manzur, C., Cabello, G., and Chornik, B. (2014). Synthesis and characterization of thin molybdenum oxide films prepared from molybdenum dioxo tropolonate precursors by photochemical metal-organic deposition (PMOD) and its evaluation as ammonia gas sensors. *Journal of Non-Crystalline Solids*, *387*, 21–27. http://doi.org/10.1016/j.jnoncrysol.2013.12.009

[54] Gao, J., Perkins, C. L., Luther, J. M., Hanna, M. C., Chen, H.-Y., Semonin, O. E.,Beard, M. C. (2011). n-Type Transition Metal Oxide as a Hole Extraction Layer in PbS Quantum Dot Solar Cells. *Nano Letters*, *11*, 3263–3266. http://doi.org/10.1007/978-1-4614-8148-5

[55] Kovalchuk, I. A. V. and M. V. (2001). Theory and applications of x-ray standing waves in real crystals. *Reports on Progress in Physics*, *64*(9), 1009. http://doi.org/10.1088/0034-4885/64/9/201

[56] Wang, B. Y. H. (1994). Step Size, Scanning Speed and Shape of X-ray Diffraction Peak, *JAC*, 716–721. http://doi.org/10.1107/S002188989400186X

[57] H. Kuzmany. (2009). Solid-State Spectroscopy. Springer. http://doi.org/10.1007/978-3-642-01479-6

[58] Manasreh, M.O. (2012). Introduction to Nanomaterials and Devices. Wiley, 217-230

[59] Alim, K. A., Fonoberov, V. A., Balandin, A. A., Alim, K. A., Fonoberov, V. A., & Balandin, A. A. (2016). Origin of the optical phonon frequency shifts in ZnO quantum dots Origin of the optical phonon frequency shifts in ZnO quantum dots, *Applied Physics, 053103*(2005), 1–4. http://doi.org/10.1063/1.1861509

[60] M. Dieterle and G. Mestl. (2001). Part II.y Resonance Raman spectroscopic characterization of the molybdenum oxides Mo4O11 and MoO2. Phys. Chem. 822-826. http://doi.org/10.1038/285176a0

Appendix A: Description of Research for Popular Publication

A new generation of display technology such as TVs, cell phones, and tablets depends on the possibility to produce light with highly saturated color. The light generated by quantum dots is saturated enough to be the core of ultra-high definition (HD) displays. Up to now, Samsung and Sony have production lines for TVs with ultra HD images based on quantum dots technology. In addition, there is another direction for QDs marketing lighting application, but this will not be in the near future because more improvement is needed for the efficiency of these devices. Quantum dots LEDs are the devices that utilize the unique optical properties of QDs. In general, these devices consist of an emissive layer made of quantum dots sandwiched between two metal oxide layers function as hole transport layer and electron transport layer. To ensure a saturated color produced by these devices, the quantum dots should have an emission spectrum that is narrow enough to reflect a high quality saturated color. A narrow spectrum is a result of the QD monodispersity. In this thesis, a QD-LED was fabricated at room temperature using a QDs produced by colloidal synthesis. The emission spectrum of the QDs has a FWHM of 45 nm centered at 515 nm, which results in a device with a saturated color. This work is an attempt to validate the theoretical principles behind QD-LEDs following and optimizing the methods of the materials synthesis deposition.

QD-LEDs consist of three main layers: electron transport layer (ETL), hole transport layer (HTL), and emissive layer which is the quantum dot layer. Motivated by low cost and the high electrochemical stability that inorganic materials have, ZnO and NiO were chosen to form the ETL and the HTL of the device, respectively. The electrochemical stability is an important trait for long life device which otherwise might experience a degradation in their structure.

There are still hurdles that need to be overcomes in order for this new technology to enter the market starting with having better understating to the working principles of these devices.

Appendix B: Executive Summary of Newly Created Intellectual Property

There was no newly created intellectual property in this research.

Appendix C: Potential Patent and Commercialization Aspects of listed Intellectual Property Items

C.1 Patentability of Intellectual Property.

Not applicable. There was no newly created intellectual property in this research.

C.2 Commercialization Prospects

Not applicable. There was no newly created intellectual property in this research.

C.3 Possible Prior Disclosure of IP

Not applicable. There was no newly created intellectual property in this research.

Appendix D: Broader Impact of Research

D.1 Applicability of Research Methods to Other Problems

All the methods used to produce materials in this research can be used in other applications. The same metal oxide layers are used with solar cells and biosensors. The spin-coating used to deposit the QD-LED layers is also used to deposit layers for photodetectors and solar cells.

D.2 Impact of Research Results on U.S. and Global Society

A direct significant impact is unlikely to happen in the short term, but the large-scale production of QD-LEDs will have an impact on the TV and cell phones industries as well as the industry of traditional light bulbs. As in any new technology, some industries will adapt the new venture and others will fade. If QD-LEDs become competitive in the lighting market, the impact will affect the electricity suppliers and bulb factories as well as any party that has ties to these two.

D.3 Impact of Research Results on the Environment

The marketing of QD LEDs in lighting applications at a large scale will have an impact on the environment. Almost 20% of the consumed electrical energy goes to lighting, which is about 2,650 TWh [1]. The produced carbon dioxide emitted from such amount of energy was two billion tons in 2010 [1]. Because of the low efficiency of incandescent bulbs, only 10 percent of the energy used is actually converted to light while the other 90 percent is dissipated as heat [1]. On the other hand, fluorescent lamps waste 70-80% from the energy is the [1]. Driven by the evolving awareness of the carbon emission impact, great efforts have been spent to find alternative efficient light sources. LEDs represent the most efficient and longest lifetime. Currently, the common types of LEDs are those which are based on quantum well InGaN/GaN.

Despite the high efficiency of these LEDs, the fabrication cost is high and the devices suffer from defects that constrain their performance. Organic LEDs OLEDs offer low fabrication cost compared with the conventional LEDs, but the conversation efficiency is still low. The third type of LEDs, presented in this thesis overcomes the cost problem and the lifetime but it also needs more research to increase the efficiency before the market can grow.

References

[1] Bae, W.K., Brovelli, S. and Klimov, V.I. (2013) 'Spectroscopic insights into the performance of quantum dot light-emitting diodes', *MRS Bulletin*, 38(9), pp. 721–730. http://doi.org/10.1557/mrs.2013.182

Appendix E: Microsoft Project for MS MicroEP Degree Plan

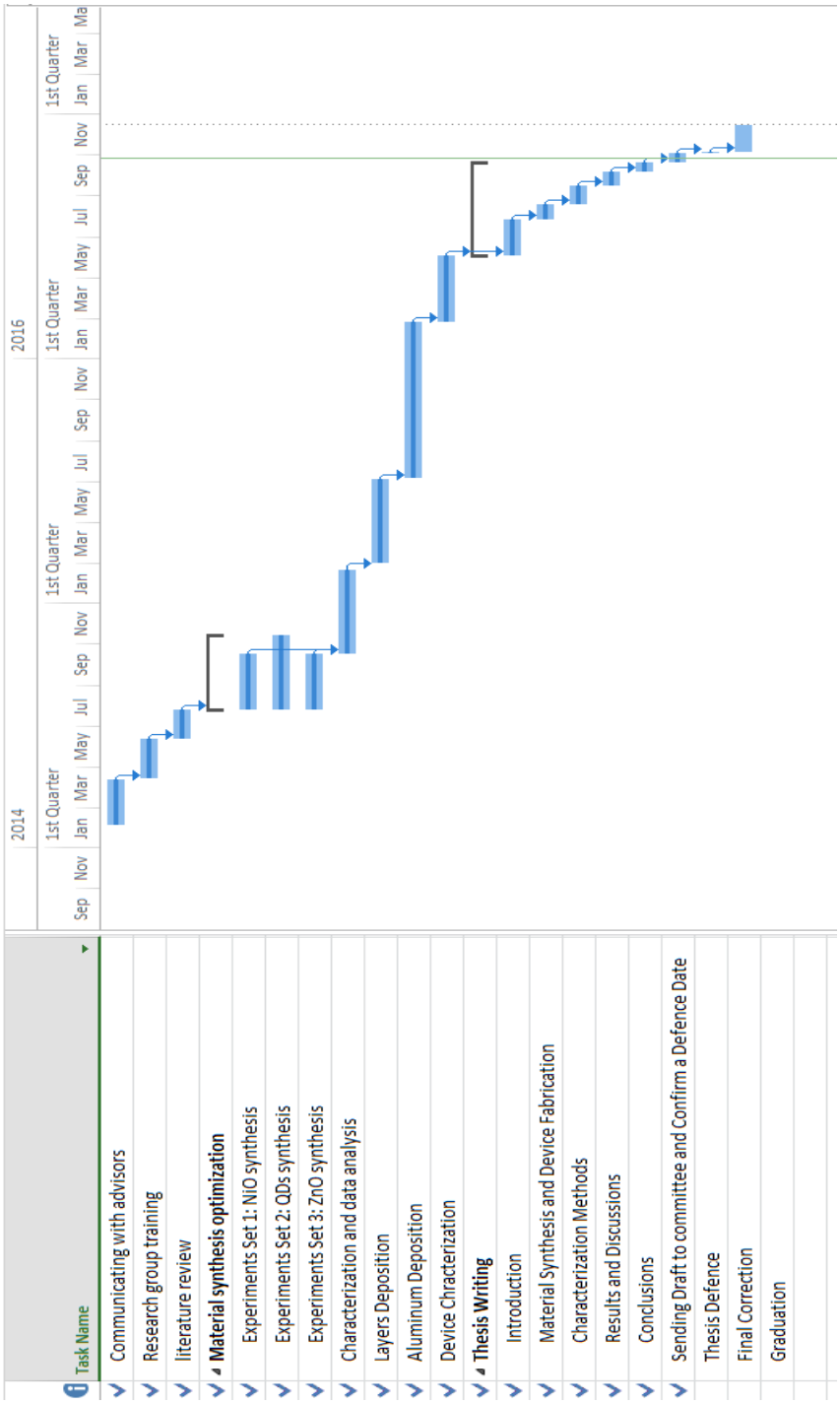

Appendix F: Identification of All Software Used in Research and Thesis Generation

Computer #1:

Model Number: Dell OptiPlex 790
Serial Number: DNH66V1
Location: Bell Engineering, Student Computer Terminal Room
Owner: Prof. Omar Manasreh

Software #1:

Name: Microsoft Office 2013
Purchased by: Department of Electrical Engineering, University of Arkansas

Software #2:

Name: MATLAB R2014b
Purchased by: Department of Electrical Engineering, University of Arkansas

Software #3:

Name: Mendeley (v. 1.9.2)
Purchased By: Haider Salman
License: Freeware

Software #4:

Name: Origin (v.8.6)
Purchased by: Prof. Omar Manasreh

Appendix G: All Publications Published, Submitted, and Planned

Publications published

Vasan, R., Salman, H. and Manasreh, M.O. (2016). All inorganic quantum dot light emitting devices with solution processed metal oxide transport layers. *MRS Advances*, pp. 305-310 http://doi.org/10.1557/adv.2016.129